

A Geometric Approach to Strongly Correlated Bosons: From N -Representability to the Generalized BEC Force

Chih-Chun Wang^{1, 2} and Christian Schilling^{1, 2, *}

¹Department of Physics, Arnold Sommerfeld Center for Theoretical Physics,

Ludwig-Maximilians-Universität München, Theresienstr. 37, 80333 Munich, Germany

²Munich Center for Quantum Science and Technology (MCQST), Schellingstr. 4, 80799 Munich, Germany

(Dated: January 6, 2026)

Building on recent advances in reduced density matrix theory, we develop a geometric framework for describing strongly correlated lattice bosons. We first establish that translational symmetry, together with a fixed pair interaction, enables an exact functional formulation expressed solely in terms of momentum occupation numbers. Employing the constrained-search formalism and exploiting a geometric correspondence between N -boson configuration states and their one-particle reduced density matrices, we derive the general form of the ground-state functional. Its structure highlights the omnipresent significance of one-body N -representability: (i) the domain is exactly determined by the N -representability conditions; (ii) at its boundary, the gradient of the functional diverges repulsively, thereby generalizing the recently discovered Bose-Einstein condensate (BEC) force; and (iii) an explicit expression for this boundary force follows directly from geometric arguments. These key results are demonstrated analytically for few-site lattice systems, and we illustrate the broader significance of our functional form in defining a systematic hierarchy of functional approximations.

I. INTRODUCTION

Describing quantum many-body systems remains one of the central challenges in physics, chemistry, and materials science. The exponential growth of the Hilbert space with particle number renders exact wave-function-based approaches intractable beyond very small systems, while the wave function itself contains far more information than is typically required. Density functional theory (DFT) [1, 2] circumvents this difficulty by replacing the wave function with the particle density $n(\vec{r})$ as the primary variable and has become an indispensable *ab initio* method in electronic structure theory [3–5]. However, DFT provides only indirect access to correlation effects and therefore often lacks predictive power for strongly correlated systems.

One-particle reduced density matrix functional theory (RDMFT) offers a conceptually richer framework by using the full one-particle reduced density matrix (1RDM) $\hat{\gamma}$ as its fundamental variable [6–8]. The 1RDM yields the kinetic energy exactly and reflects correlation directly through fractional occupation numbers, making RDMFT particularly suitable for the description of strongly correlated systems. Over the past decades, RDMFT has undergone substantial development through advances in its theoretical foundations and scope [6–21], the understanding of general properties of the universal functional [22–24], the derivation of exact functionals for small systems [19, 25–28], the construction of approximate functionals [28–50], and increasingly sophisticated algorithmic implementations [51–56].

Despite these advances, the full potential of RDMFT remains unrealized. In particular, a comprehensive un-

derstanding of the structure of the universal functional, the consistent incorporation of N -representability, and the systematic construction of controlled approximations is still lacking. This gap is especially pronounced for bosonic systems: although interacting bosons play a central role in modern quantum many-body physics [57], bosonic RDMFT has only very recently been established at a formal level [15, 28]. In this context, RDMFT would be particularly well suited, as it provides direct access to the momentum density, determined through the time-of-flight method in experiments [58], and allows for a universal characterization of Bose-Einstein condensation through the Penrose-Onsager criterion, applicable to both homogeneous and inhomogeneous systems [59]. It is precisely in this broader context that ultracold atomic gases have emerged as one of the central platforms of modern quantum many-body physics, providing an exceptionally clean and controllable platform for exploring these phenomena [57, 58, 60–65], with optical lattice realizations enabling controlled studies of superfluid-Mott insulator physics [66–69].

In this work, we close this gap by showing that spatial symmetry, N -representability, and the geometry of quantum states jointly determine the structure of the universal interaction functional for lattice bosons. As anticipated in Fig. 1, incorporating translational symmetry into RDMFT leads to a decisive simplification: the functional variable reduces to the momentum occupation number vector. We demonstrate that the geometry of the functional domain governs the functional form and enforces a universal boundary behavior, namely a repulsive divergence of the functional gradient. This generalized BEC force extends earlier results from the BEC vertex to arbitrary boundary points, is derived here in closed analytical form, and reveals how N -representability and state-space geometry constrain all admissible functionals, providing a principled route toward their systematic

* c.schilling@lmu.de

approximation.

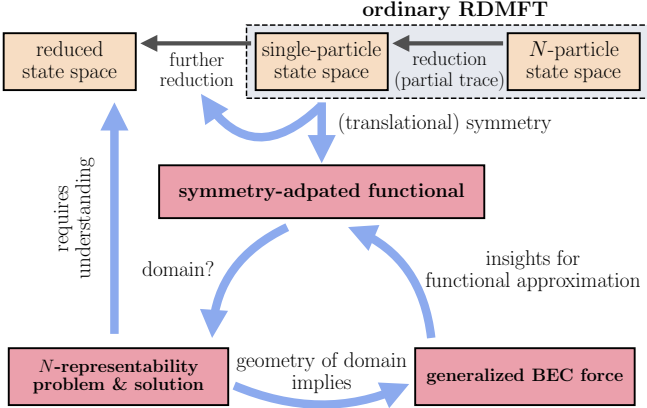


FIG. 1. Conceptual overview of the symmetry-adapted functional-theoretical framework developed in this work. See text for details.

This paper is organized as follows. In Sec. II, we review the general framework of RDMFT and explain how translational symmetry simplifies the functional domain. Section III presents a complete characterization of this domain, with an emphasis on small lattice systems. In Sec. IV, we derive the general form of the ground-state functional and analyze its geometric structure. Section V reveals the generalized BEC force, while Sec. VI illustrates our findings for a Bose-Hubbard model and outlines a geometrically guided strategy for constructing functional approximations.

II. NOTATION AND CONCEPTS

A. Recap and Rationalization of RDMFT

Although bosonic systems are our primary focus, we briefly review in this section the basic elements of one-particle reduced density-matrix functional theory (RDMFT) for both bosonic and fermionic systems. This broader perspective enables a transparent comparison between the two cases. In particular, it allows us to identify structural features of functional theories that are distinctive to bosons and either absent or much less pronounced in the fermionic setting, where functional approaches are comparatively more mature and well established.

Throughout this paper, \mathcal{H}_1 and \mathcal{H}_N denote the single-particle and N -particle Hilbert spaces, respectively. The many-particle Hilbert space is given by the symmetrized tensor product $\mathcal{H}_N = \text{Sym}^N \mathcal{H}_1$ for bosons and by the antisymmetrized tensor product $\mathcal{H}_N = \bigwedge^N \mathcal{H}_1$ for fermions, reflecting the corresponding symmetry under particle exchange.

Functional theories are particularly effective because they do not target the ground state of a single, isolated

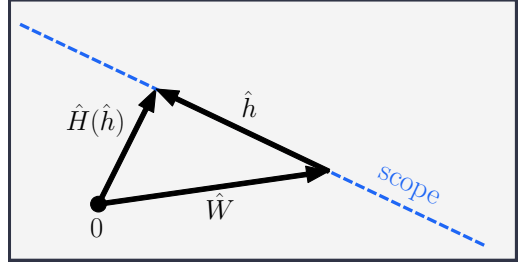


FIG. 2. Schematic illustration of the concept of *scope*: a functional theory is associated with a family of Hamiltonians $\hat{H}(\hat{h}) = \hat{h} + \hat{W}$, where \hat{h} varies within a physically relevant real vector space of Hermitian operators determined by the problem class and its symmetries. The set of admissible Hamiltonians $\{\hat{H}(\hat{h})\}$ thus forms an affine space (blue dashed line), referred to as the scope of the functional theory.

system, but rather provide a unified description of an entire class of systems that share a common physical structure [19]. In many-body physics and quantum chemistry, such classes naturally arise through experimentally or physically controllable parameters. In electronic-structure theory, for instance, the Hamiltonian depends on the external potential $v(\vec{r})$ determined by the nuclear configuration, while in ultracold-atom experiments the parameters of the trapping potential, and hence the one-particle term of lattice models such as the Bose-Hubbard Hamiltonian, can be tuned [66, 67]. Functional theories take advantage of this shared structure to treat all members of the class on equal footing.

This observation motivates the introduction of the concept of *scope*, which constitutes one of the key conceptual ingredients of the present work. The scope specifies the class of Hamiltonians to which a given functional theory applies and thereby clarifies, in a systematic and conceptually transparent manner, what the theory is designed to describe and what it can be expected to deliver.

In RDMFT, one considers Hamiltonians of the form

$$\hat{H}(\hat{h}) = \hat{h} + \hat{W}, \quad (1)$$

where \hat{h} denotes a general one-particle operator, typically comprising kinetic and external potential terms, and \hat{W} is a fixed interaction operator. Depending on the physical context, \hat{W} may represent a contact interaction in ultracold atomic gases, a Hubbard-type on-site interaction in solid-state models, or the Coulomb interaction in quantum chemistry. The admissible Hamiltonians $\{\hat{H}(\hat{h})\}$ therefore form an affine subspace of the space of Hermitian operators on \mathcal{H}_N , as illustrated schematically in Fig. 2. Specifying this affine space, i.e. the scope, is the first essential ingredient of the functional theory.

The second ingredient is a variational principle. For ground-state problems, this role is played by the Rayleigh-Ritz variational principle, which yields the ground-state energy

$$E(\hat{h}) = \min_{|\Psi\rangle} \langle \Psi | \hat{h} + \hat{W} | \Psi \rangle. \quad (2)$$

Exploiting the common splitting $\hat{H}(\hat{h}) = \hat{h} + \hat{W}$, the expectation value separates naturally into a one-particle and an interaction contribution. Introducing the one-particle reduced density operator (1RDM) associated with an N -particle mixed or pure state $\hat{\Gamma}$,

$$\hat{\gamma} \equiv N \text{Tr}_{N-1}(\hat{\Gamma}), \quad (3)$$

one may rewrite the variational problem in terms of $\hat{\gamma}$ and arrive at the constrained-search formulation of RDMFT [19, 70, 71]. In particular, the *pure-state constrained search functional* [70]

$$\mathcal{F}[\hat{\gamma}] \equiv \min_{|\Psi\rangle \mapsto \hat{\gamma}} \langle \Psi | \hat{W} | \Psi \rangle \quad (4)$$

encodes the interaction contribution universally across the entire scope. The ground-state energy corresponding to any Hamiltonian $\hat{H}(\hat{h})$ within the scope is then obtained by minimizing $\text{Tr}(\hat{h}\hat{\gamma}) + \mathcal{F}[\hat{\gamma}]$ over all admissible $\hat{\gamma}$, a result that follows directly from the Rayleigh-Ritz variational principle [6, 19, 70, 71].

This construction makes explicit a central message of the present work: functional theories arise from the interplay of two fundamental ingredients: the specification of a scope and the choice of a variational principle. Once these ingredients are fixed, the structure of the functional theory follows in a systematic and largely theory-independent manner.

The minimization in Eq. (4) is well defined only for one-particle density operators $\hat{\gamma}$ that originate from pure N -particle states, a condition known as (*pure-state*) N -*representability*. The domain of the pure functional \mathcal{F} is thus the set of all pure-state N -representable 1RDMs. For fermions, this set is restricted by the generalized Pauli constraints on the natural occupation numbers [72–75]. For bosons, by contrast, every one-particle density operator with trace N is pure-state N -representable [28, 76], which substantially simplifies the formulation and use of bosonic RDMFT.

From the scope-based perspective outlined above, it becomes transparent how functional theories can be extended beyond ground states to target excited states. Since the scope, i.e., the class of admissible Hamiltonians, remains unchanged, such extensions are achieved by simply modifying the second fundamental ingredient of the theory, namely the variational principle. Replacing the Rayleigh-Ritz principle by an ensemble variational principle based on weighted energies $E_{\mathbf{w}} \equiv \sum_i w_i E_i$ with non-increasing auxiliary weights \mathbf{w} [77, 78] yields ensemble functionals that describe low-lying excitations. This approach underlies the formulation of \mathbf{w} -ensemble RDMFT [13, 16] and closely parallels developments in ensemble density functional theory [79–90]. As a consequence, many of the conceptual insights and practical results derived in this work can be obtained in a closely analogous manner within ensemble formulations beyond the ground-state setting.

B. Incorporating Translational Symmetry

In the context of the present work motivated by translationally invariant lattice models for bosonic quantum matter it is advantageous to incorporate translational symmetry explicitly into the functional framework. More generally, a systematic scope-based approach to incorporating symmetries into functional theories has been developed at an abstract level and explicitly realized for spin symmetries in Refs. [91, 92]. Here, we demonstrate that this framework can be adapted to the equally important case of translational symmetry. As we will show, translational invariance has two key consequences: it induces a decomposition of the many-particle Hilbert space into independent symmetry sectors that can be addressed individually within a functional-theoretical framework, and it allows for a simplification of both the functional variable and its domain. Exploiting these aspects, we construct a symmetry-adapted version of RDMFT tailored to translationally invariant systems.

We consider N bosons on a one-dimensional lattice with d sites and periodic boundary conditions. Translational invariance implies that the Hamiltonian commutes with lattice translations, making the momentum representation particularly convenient. Let $\{|k\rangle\}_{k=0}^{d-1}$ denote the single-particle momentum eigenstates. An orthonormal basis of the N -particle Hilbert space is then given by the bosonic occupation-number states

$$|n_0, \dots, n_{d-1}\rangle = \prod_{k=0}^{d-1} \frac{(\hat{b}_k^\dagger)^{n_k}}{\sqrt{n_k!}} |0\rangle, \quad (5)$$

with fixed particle number $\sum_{k=0}^{d-1} n_k = N$, where \hat{b}_k^\dagger creates a boson with momentum k and $|0\rangle$ denotes the vacuum state.

Each such configuration is an eigenstate of the translation operator \hat{g} , with eigenvalue determined by the total momentum,

$$\hat{g} |n_0, \dots, n_{d-1}\rangle = e^{\frac{2\pi i}{d} \sum_{k=0}^{d-1} k n_k} |n_0, \dots, n_{d-1}\rangle. \quad (6)$$

As a result, the N -particle Hilbert space decomposes into d symmetry sectors labeled by the conserved total momentum $P = 0, 1, \dots, d-1$,

$$\mathcal{H}_N = \bigoplus_{P=0}^{d-1} \mathcal{H}_N^{(P)}, \quad (7)$$

with

$$\mathcal{H}_N^{(P)} = \text{span}_{\mathbb{C}} \left\{ |n_0, \dots, n_{d-1}\rangle \mid \sum_{k=0}^{d-1} k n_k \equiv P \pmod{d} \right\}. \quad (8)$$

As a simple illustration, for $N = 3$ bosons on $d = 3$ lattice sites the sectors $P = 0, 1, 2$ are spanned by $\{|3, 0, 0\rangle, |0, 3, 0\rangle, |0, 0, 3\rangle, |1, 1, 1\rangle\}$, $\{|2, 1, 0\rangle, |0, 2, 1\rangle, |1, 0, 2\rangle\}$, and $\{|1, 2, 0\rangle, |0, 1, 2\rangle, |2, 0, 1\rangle\}$, respectively.

Since the Hamiltonian is block-diagonal with respect to the decomposition (7), variational ground-state methods can be applied separately in each symmetry sector $\mathcal{H}_N^{(P)}$. This sector-wise formulation yields not only the global ground state as the minimum over all P , but also the energetic minimum within each individual sector, while significantly reducing numerical cost. More importantly, in functional-theoretical frameworks it is essential: mixing different symmetry sectors leads to symmetry contamination, a well-known and severe pathology of practical functional approximations, most prominently encountered in the treatment of spin symmetries.

The second step in constructing the symmetry-adapted functional theory exploits the restriction imposed by translational invariance on the one-particle Hamiltonian. In this setting, the one-particle operator \hat{h} reduces to a generalized kinetic-energy operator \hat{t} that is diagonal in the momentum representation,

$$\hat{h} \equiv \hat{t} = \sum_{k=0}^{d-1} t_k \hat{b}_k^\dagger \hat{b}_k. \quad (9)$$

Here, the coefficients t_k characterize a general single-particle dispersion relation whose rate and range can be tuned in ultracold atom experiments [93, 94], allowing for a broad class of effective kinetic energy operators. As a consequence, the one-particle energy

$$\text{Tr}(\hat{h}\hat{\gamma}) = \vec{t} \cdot \vec{n} \quad (10)$$

depends only on the momentum occupation numbers

$$n_k \equiv \langle \Psi | \hat{b}_k^\dagger \hat{b}_k | \Psi \rangle = \langle k | \hat{\gamma} | k \rangle, \quad (11)$$

which form the vector $\vec{n} = (n_0, \dots, n_{d-1})^\top$, while $\vec{t} = (t_0, \dots, t_{d-1})^\top$ collects the corresponding single-particle energies. Thus, in the presence of translational symmetry, the full 1RDM contains redundant information for the variational problem.

These observations lead directly to the introduction of a symmetry-adapted pure functional in a fixed momentum sector P ,

$$\mathcal{F}^{(P)}[\vec{n}] \equiv \min_{\mathcal{H}_N^{(P)} \ni |\Psi\rangle \mapsto \vec{n}} \langle \Psi | \hat{W} | \Psi \rangle, \quad (12)$$

where $|\Psi\rangle \mapsto \vec{n}$ denotes the constraint $\langle \Psi | \hat{b}_k^\dagger \hat{b}_k | \Psi \rangle = n_k$ for all k . The domain of $\mathcal{F}^{(P)}$ consists of all momentum-occupation vectors \vec{n} that are compatible with a pure N -boson state in the sector $\mathcal{H}_N^{(P)}$; this representability problem is addressed in Sec. III.

With the definition (12), the ground-state energy of $\hat{h} + \hat{W}$ within a fixed symmetry sector $\mathcal{H}_N^{(P)}$ is obtained as

$$E^{(P)} = \min_{\vec{n} \in \text{dom } \mathcal{F}^{(P)}} (\vec{t} \cdot \vec{n} + \mathcal{F}^{(P)}[\vec{n}]), \quad (13)$$

in direct analogy to standard RDMFT. For each P , the functional $\mathcal{F}^{(P)}$ is universal in the sense that it depends

only on the interaction \hat{W} and not on the specific kinetic-energy operator. This universality highlights the economical nature of functional theories: once approximations to $\mathcal{F}^{(P)}$ are developed for a given interaction, they can be reused across an entire class of systems, in stark contrast to wave function-based approaches.

Finally, we note that translational invariance of the interaction operator \hat{W} implies that it is likewise block-diagonal with respect to the momentum sectors $\mathcal{H}_N^{(P)}$. For a general two-body interaction, this block structure is reflected in momentum conservation and can be expressed in second quantization as

$$\hat{W} = \sum_{k_1, k_2, k_3, k_4} W_{k_1 k_2 k_3 k_4} \delta_{k_1+k_2, k_3+k_4} \hat{b}_{k_1}^\dagger \hat{b}_{k_2}^\dagger \hat{b}_{k_3} \hat{b}_{k_4}, \quad (14)$$

where the Kronecker delta is understood modulo d . A paradigmatic example is the one-dimensional Bose-Hubbard model with periodic boundary conditions, for which

$$\hat{W} = \frac{1}{d} \sum_{k_1, k_2, k_3, k_4} \delta_{k_1+k_2, k_3+k_4} \hat{b}_{k_1}^\dagger \hat{b}_{k_2}^\dagger \hat{b}_{k_3} \hat{b}_{k_4}, \quad (15)$$

corresponding in position space to an on-site interaction $\sum_{i=1}^d \hat{n}_i(\hat{n}_i - 1)$.

The analysis and results presented in this section extend straightforwardly to higher-dimensional lattices. For a three-dimensional periodic lattice, the momentum label k is replaced by a vector $\vec{k} = (k_x, k_y, k_z)$ with $k_\alpha = 0, \dots, d_\alpha - 1$, and the symmetry sectors are labeled by the conserved total momentum vector \vec{P} . All definitions and results carry over directly under this replacement. Similarly, spinful bosons can be treated by augmenting the momentum label \vec{k} with a spin (or polarization) quantum number σ , corresponding to a fixed quantization axis. In this way, the framework presented here applies equally to systems with arbitrary spatial and internal symmetries.

III. DOMAIN OF THE FUNCTIONAL AND ITS GEOMETRIC FEATURES

The goal of this section is to determine the domain of the symmetry-adapted functional $\mathcal{F}^{(P)}$ in each symmetry sector $\mathcal{H}_N^{(P)}$, i.e., to characterize the set of momentum occupation number vectors \vec{n} that can arise from an N -particle pure state $|\Psi\rangle$ with total momentum P . Understanding this domain is essential, as it encodes purely kinematic constraints and will later be shown to strongly shape the universal interaction functionals $\mathcal{F}^{(P)}$.

The occupation numbers necessarily satisfy $\sum_k n_k = N$ and $n_k \geq 0$, which define a $(d-1)$ -simplex in \mathbb{R}^d . Once the total momentum P is fixed, however, these conditions are generally not sufficient. For most choices of (d, N, P) , the actual domain $\text{dom } \mathcal{F}^{(P)}$ is a strict subset of this simplex and takes the form of a convex polytope that can

be visualized as arising from additional linear constraints near certain vertices. While these constraints delimit the admissible region at the kinematic level, we will show in Sec. V that, for concrete systems, the universal interaction functional associated with a given interaction \hat{W} generates a *diverging repulsive force* on the ground-state occupation number vector \vec{n} near the boundary of the domain. This observation provides the central motivation for analyzing the geometry of $\text{dom } \mathcal{F}^{(P)}$ in detail.

In order to characterize the domain of $\mathcal{F}^{(P)}$ in a precise geometric way, we recall that a *convex combination* of vectors is a linear combination with nonnegative coefficients summing to one, and that the *convex hull* of a collection of vectors is the set of all such convex combinations.

Theorem 1. *Consider a one-dimensional system of N bosons on d lattice sites. For each value of the total momentum $P = 0, \dots, d-1$, the domain of $\mathcal{F}^{(P)}$ is*

$$\text{conv} \left\{ \vec{n} \in \mathbb{N}_0^d \mid \sum_{k=0}^{d-1} n_k = N, \sum_{k=0}^{d-1} k n_k \equiv P \pmod{d} \right\}, \quad (16)$$

i.e., the convex hull of the occupation number vectors \vec{n} of all configuration states $|\vec{n}\rangle$ (5) with total momentum P .

Proof. For any N -particle state $|\Psi\rangle$ with momentum P , i.e., $|\Psi\rangle \in \mathcal{H}_N^{(P)}$, we have $|\Psi\rangle = \sum_{\alpha=1}^{\dim \mathcal{H}_N^{(P)}} c_\alpha |\vec{n}^{(\alpha)}\rangle$, where each $\vec{n}^{(\alpha)}$ satisfies $\sum_{k=0}^{d-1} k n_k^{(\alpha)} \equiv P \pmod{d}$. Thus the momentum occupation number vector \vec{n} of $|\Psi\rangle$ is given by

$$\begin{aligned} n_k &= \langle \Psi | \hat{b}_k^\dagger \hat{b}_k | \Psi \rangle = \sum_{\alpha, \beta} c_\alpha^* c_\beta \langle \vec{n}^{(\alpha)} | \hat{b}_k^\dagger \hat{b}_k | \vec{n}^{(\beta)} \rangle \\ &= \sum_{\alpha} |c_\alpha|^2 n_k^{(\alpha)}, \end{aligned} \quad (17)$$

where we have used $\langle \vec{n}^{(\alpha)} | \hat{b}_k^\dagger \hat{b}_k | \vec{n}^{(\beta)} \rangle = n_k^{(\alpha)} \delta_{\alpha\beta}$. Inspecting Eq. (17), we immediately see that the occupation number vector \vec{n} sweeps through the entire convex hull of $\{\vec{n}^{(\alpha)}\}$ as the wave-function coefficients $\{c_\alpha\}$ are varied. \square

In words, Theorem 1 shows that the domain of the functional is a convex polytope generated as convex combinations by the occupation number vectors of all configuration-number states with fixed total momentum. The statement extends straightforwardly to spatial dimensions larger than one, where the domain is given by the convex hull of all configuration-number states $|\vec{n}\rangle$ with fixed total momentum vector \vec{P} . Moreover, since the domain is convex and the map $|\Psi\rangle\langle\Psi| \mapsto \vec{n}$ is linear, the same polytope is obtained if one considers all ensemble states with support on \mathcal{H}_N^P rather than just the pure states $|\Psi\rangle\langle\Psi|$.

To illustrate these general results, we first consider the case of $d = 2$ lattice sites. The N -particle

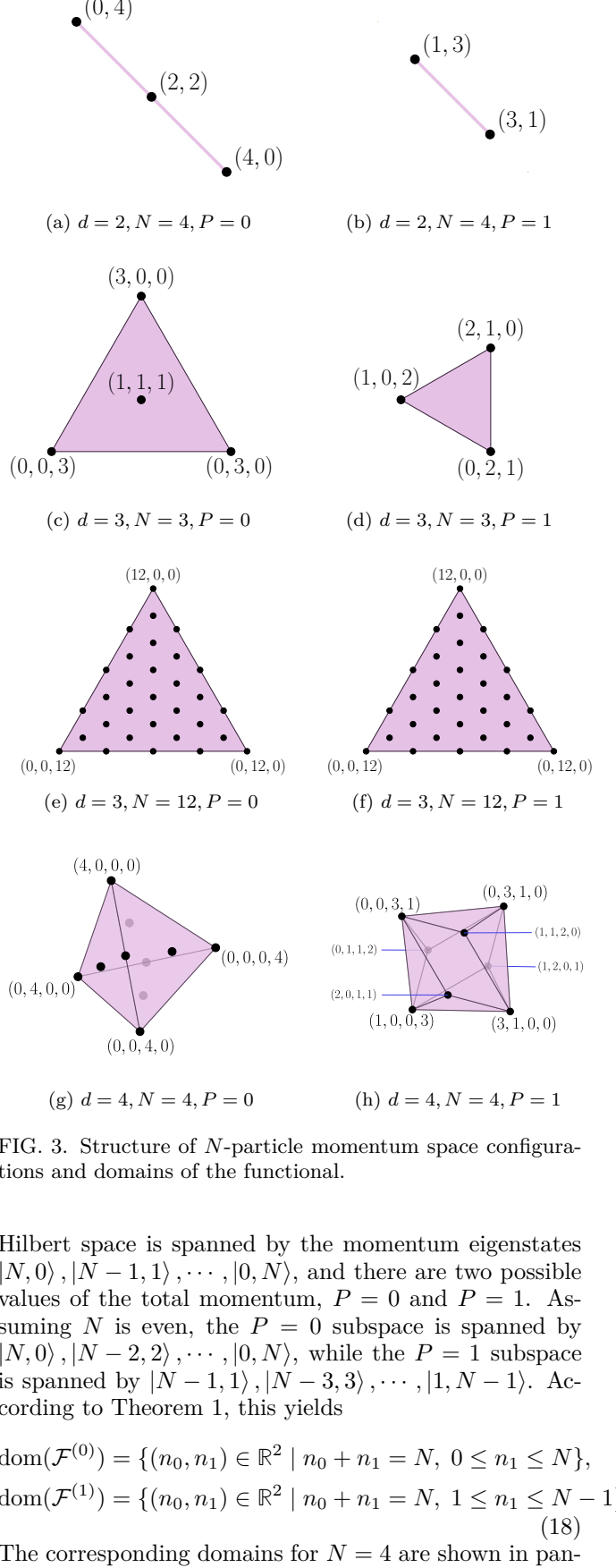


FIG. 3. Structure of N -particle momentum space configurations and domains of the functional.

Hilbert space is spanned by the momentum eigenstates $|N, 0\rangle, |N-1, 1\rangle, \dots, |0, N\rangle$, and there are two possible values of the total momentum, $P = 0$ and $P = 1$. Assuming N is even, the $P = 0$ subspace is spanned by $|N, 0\rangle, |N-2, 2\rangle, \dots, |0, N\rangle$, while the $P = 1$ subspace is spanned by $|N-1, 1\rangle, |N-3, 3\rangle, \dots, |1, N-1\rangle$. According to Theorem 1, this yields

$$\begin{aligned} \text{dom}(\mathcal{F}^{(0)}) &= \{(n_0, n_1) \in \mathbb{R}^2 \mid n_0 + n_1 = N, 0 \leq n_1 \leq N\}, \\ \text{dom}(\mathcal{F}^{(1)}) &= \{(n_0, n_1) \in \mathbb{R}^2 \mid n_0 + n_1 = N, 1 \leq n_1 \leq N-1\}. \end{aligned} \quad (18)$$

The corresponding domains for $N = 4$ are shown in pan-

els (a) and (b) of Fig. 3.

For general (d, N, P) , the geometry of the domain becomes more involved, as illustrated in Fig. 3. A few general observations are in order. First, whenever d divides N , the configurations $|N, 0, \dots, 0\rangle, |0, N, 0, \dots, 0\rangle, \dots$ all belong to the zero-momentum subspace, and $\text{dom } \mathcal{F}^{(0)}$ coincides with the full simplex spanned by these states (see panels (a), (c), (e), and (g)). Second, in the limit $N \rightarrow \infty$ at fixed d and P , the vertices of the simplex approach, relative to N , the nearest admissible occupation number vectors with total momentum P , so that the domain approaches a simplex asymptotically (see panel (f)).

Finally, panels (a), (c), (e), and (f) of Fig. 3 highlight a distinctive feature of the bosonic setting in contrast to fermions [22]: the occupation number vectors of configuration states $|\vec{n}\rangle \in \mathcal{H}_N^{(P)}$ are not necessarily extremal points of the domain but form a regular lattice that may also populate its interior. As will become clear in Sec. V, both the shape of the domain and the distribution of occupation number vectors of the configuration states within it play an essential role in determining the behavior of the functional near the boundary.

IV. FORM OF UNIVERSAL FUNCTIONAL

In usual RDMFT without explicitly incorporating symmetries, as outlined in Sec. II A, various approximate universal functionals have been proposed in the literature, mostly for electronic systems [29, 38, 51, 95–97], with exact analytical results available only for a few specific model systems [27, 28]. The systematic exploitation of spatial symmetries in RDMFT has so far been limited. For arbitrary translationally invariant fermionic lattice models, this was carried out in a comprehensive manner in Ref. [22], where the pure functional \mathcal{F} was shown to depend sensitively on the geometry of its domain. The aim of this section is to extend these ideas to *bosonic* systems and to accommodate arbitrary kinetic-energy operators, in line with modern ultracold-atom experiments, where both the amplitudes and the range of hopping processes can be tuned [93, 94]. From now on, to simplify the notation, we drop the superscript P in $\mathcal{F}^{(P)}$.

As is apparent in Sec. III, the domain of \mathcal{F} is a subset of the hyperplane $\{\vec{n} \in \mathbb{R}^n \mid \sum_k n_k = N\}$ bounded by a list of $J = J(d, N, P)$ affine constraints

$$D^{(j)}(\vec{n}) = \vec{\kappa}^{(j)} \cdot \vec{n} + \mu^{(j)} \geq 0, \quad (19)$$

where $j = 1, \dots, J$ labels the facets. Note that there is some ambiguity in the choice of $\vec{\kappa}^{(j)}$ and $\mu^{(j)}$. For instance, scaling them by a positive constant, or replacing them with $\vec{\kappa}^{(j)} \rightarrow \vec{\kappa}^{(j)} + (\nu, \dots, \nu)$ and $\mu^{(j)} \rightarrow \mu^{(j)} - \nu N$ for any ν , results in an equivalent constraint. This ambiguity, however, does not affect any physical result in this section.

As an illustrative example, consider $N = 3$ bosons on $d = 3$ lattice sites with total momentum $P = 1$ (panel

(d) of Fig. 3). The spanning states are $\vec{n}^{(1)} = |2, 1, 0\rangle$, $\vec{n}^{(2)} = |0, 2, 1\rangle$, and $\vec{n}^{(3)} = |1, 0, 2\rangle$. The domain of the functional is given by the three inequality constraints

$$\begin{aligned} D^{(1)}(\vec{n}) &= n_0 - n_2 + 1 \geq 0 \\ D^{(2)}(\vec{n}) &= n_1 - n_0 + 1 \geq 0 \\ D^{(3)}(\vec{n}) &= n_2 - n_1 + 1 \geq 0, \end{aligned} \quad (20)$$

together with the normalization condition $n_0 + n_1 + n_2 = 3$.

The key idea of our work is to express now $\mathcal{F}[\vec{n}]$ in terms of the quantities $D^{(j)}(\vec{n})$, $j = 1, \dots, J$, which geometrically measure the distance of \vec{n} (up to a multiplicative factor) from the j -th facet. We proceed in two steps. First, we treat a simplified scenario, the so-called ‘simplex setting’ (see below for a precise definition). Although a general combination of (d, N, P) does not satisfy the simplex assumption, this basic setting allows us to derive the functional in a straightforward way and to illustrate the essential features without encountering technical complications. Next, in the subsequent section, armed with the intuition obtained in the simplex setting, we will drop this assumption and derive a functional form in full generality, i.e., for arbitrary (d, N, P) .

A. The Simplex

In general, an *m-simplex* is an m -dimensional polytope which is the convex hull of its $m + 1$ vertices. In this section, we assume that the domain is a simplex with exactly $\dim \mathcal{H}_N^{(P)}$ vertices, meaning in particular that the momentum occupation number vector $\vec{n}^{(\alpha)}$ of each configuration state $|\vec{n}^{(\alpha)}\rangle$ lies on a vertex. This is a strong condition on (d, N, P) , and only specific combinations of low dimension and low particle number result in such a scenario. For example, panels (b) and (d) of Fig. 3 satisfy this assumption, while the remaining panels do not. Note that although the functional domains in panels (a), (c), (e), and (g) are geometrically simplices, they are excluded from the discussion in this section because of the additional $\vec{n}^{(\alpha)}$ vectors which are not vertices. Hereafter, the *simplex assumption* or *simplex setting* always refers to this stronger condition, rather than merely requiring the domain to be a simplex.

Let $\vec{n}^{(\alpha)}$, $\alpha = 1, \dots, \dim \mathcal{H}_N^{(P)}$, denote the list of vertices. The Hilbert space $\mathcal{H}_N^{(P)}$ is then spanned by the corresponding configuration states $|\vec{n}^{(\alpha)}\rangle$. Since for simplices there is a one-to-one correspondence between vertices and facets, the number J of facets equals $\dim \mathcal{H}_N^{(P)}$, and we use Greek letters α, β to label the constraints instead of j , as in Eq. (19). More precisely, we label the constraints such that $D^{(\alpha)} = 0$ corresponds to the facet opposite the vertex $\vec{n}^{(\alpha)}$.

To evaluate \mathcal{F} at a given occupation number vector \vec{n} , we consider a state $|\Psi\rangle = \sum_\alpha c_\alpha |\vec{n}^{(\alpha)}\rangle$ whose one-body occupations satisfy $\langle \Psi | \hat{b}_k^\dagger \hat{b}_k | \Psi \rangle = n_k$ for all k . Applying

the affine functional $D^{(\beta)}$ then to both sides of Eq. (17) yields

$$\sum_{\alpha} |c_{\alpha}|^2 D^{(\beta)}\left(\vec{n}^{(\alpha)}\right) = D^{(\beta)}(\vec{n}). \quad (21)$$

Since all vertices except $\vec{n}^{(\beta)}$ lie on the facet $D^{(\beta)} = 0$, we have $D^{(\beta)}(\vec{n}^{(\alpha)}) = L_{\alpha} \delta_{\alpha\beta}$ with $L_{\alpha} \equiv D^{(\alpha)}(\vec{n}^{(\alpha)})$. It therefore follows that

$$|c_{\beta}|^2 = \frac{D^{(\beta)}(\vec{n})}{L_{\beta}}, \quad (22)$$

which admits a direct geometric interpretation as a ratio of distances to the facets of the domain.

As a central result of our work, the interaction functional (12) in the simplex setting can thus be written explicitly as

$$\mathcal{F}[\vec{n}] = \sum_{\alpha, \beta=1}^{\dim \mathcal{H}_N^{(P)}} W_{\alpha\beta} \eta_{\alpha}^{*}(\vec{n}) \eta_{\beta}(\vec{n}) \sqrt{\frac{D^{(\alpha)}(\vec{n})}{L_{\alpha}}} \sqrt{\frac{D^{(\beta)}(\vec{n})}{L_{\beta}}}, \quad (23)$$

where $W_{\alpha\beta} \equiv \langle \vec{n}^{(\alpha)} | \hat{W} | \vec{n}^{(\beta)} \rangle$. The phase factors $\{\eta_{\alpha}(\vec{n})\}$ arise from the minimization of \mathcal{F} and depend implicitly on \vec{n} ; for specific interactions \hat{W} , they may be determined explicitly.

The key result (23) makes transparent how the geometry of the domain directly shapes the structure of the universal interaction functional, to a large extent independently of the specific interaction \hat{W} . The dependence on the occupation numbers enters exclusively through the facet distances $D^{(\alpha)}(\vec{n})$, so that the value of \mathcal{F} is governed by the relative position of \vec{n} within the domain. In particular, the square-root singularities associated with the facets already signal the pronounced influence of the boundary geometry on the behavior of the functional, a feature that will remain central beyond the simplex setting.

As an example, we consider again the setting $(d, N, P) = (3, 3, 1)$, whose domain is characterized by the inequality constraints in (20). We have $L_1 = L_2 = L_3 = 3$. Hence, Eq. (23) becomes

$$\begin{aligned} \mathcal{F}[\vec{n}] = & u + \frac{2}{3} \min_{\eta_1, \eta_2, \eta_3} w \operatorname{Re} \left[\eta_1^{*} \eta_2 \sqrt{D^{(1)}(\vec{n}) D^{(2)}(\vec{n})} \right. \\ & \left. + \eta_2^{*} \eta_3 \sqrt{D^{(2)}(\vec{n}) D^{(3)}(\vec{n})} + \eta_3^{*} \eta_1 \sqrt{D^{(3)}(\vec{n}) D^{(1)}(\vec{n})} \right], \end{aligned} \quad (24)$$

where we have assumed $W_{11} = W_{22} = W_{33} = u$ and $W_{\alpha \neq \beta} = w$, as in the Bose-Hubbard model. If $w \leq 0$, the minimization over the phases $\{\eta_{\alpha}\}$ is trivial and one finds

$$\begin{aligned} \mathcal{F}[\vec{n}] = & u - \frac{2}{3} |w| \left[\sqrt{D^{(1)}(\vec{n}) D^{(2)}(\vec{n})} \right. \\ & \left. + \sqrt{D^{(2)}(\vec{n}) D^{(3)}(\vec{n})} + \sqrt{D^{(3)}(\vec{n}) D^{(1)}(\vec{n})} \right]. \end{aligned} \quad (25)$$

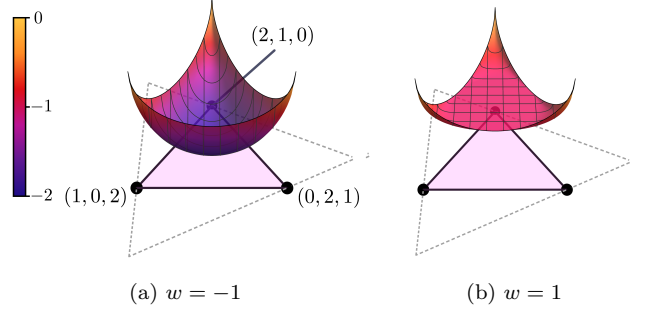


FIG. 4. The universal functional $\mathcal{F}[\vec{n}]$ for $(d, N, P) = (3, 3, 1)$ with negative (left) and positive (right) coupling parameter w . The solid triangle is the domain of \mathcal{F} , while the dashed lines outline the convex hull of $(3, 0, 0)$, $(0, 3, 0)$, and $(0, 0, 3)$. See text for details.

For w positive, the minimization over the phases $\{\eta_{\alpha}\}$ is still relatively simple. A straightforward calculation shows that $\mathcal{F}[\vec{n}] = u - w$ if $\sqrt{D^{(1)}(\vec{n})}, \sqrt{D^{(2)}(\vec{n})}, \sqrt{D^{(3)}(\vec{n})}$ satisfy the triangle inequality (i.e., $\sqrt{D^{(1)}(\vec{n})} \leq \sqrt{D^{(2)}(\vec{n})} + \sqrt{D^{(3)}(\vec{n})}$ plus cyclic permutations). Otherwise,

$$\begin{aligned} \mathcal{F}[\vec{n}] = & u + \frac{2}{3} w \left(\sqrt{D^{(1)}(\vec{n}) D^{(2)}(\vec{n})} \right. \\ & \left. - \sqrt{D^{(2)}(\vec{n}) D^{(3)}(\vec{n})} - \sqrt{D^{(3)}(\vec{n}) D^{(1)}(\vec{n})} \right) \end{aligned} \quad (26)$$

if $D^{(3)}(\vec{n}) \geq D^{(1)}(\vec{n}), D^{(2)}(\vec{n})$ (and analogously for the other cases). The functionals for $w = 1$ and $w = -1$ are shown in Fig. 4.

B. Beyond the simplex

Outside the simplex setting, i.e., whenever the domain is not a simplex with $\dim \mathcal{H}_N^{(P)}$ vertices, the coefficients $\{|c_{\alpha}|^2\}$ can no longer be reconstructed uniquely from the facet distances $\{D^{(j)}(\vec{n})\}$, in contrast to the situation in Eq. (22). Instead, the quantities $D^{(j)}(\vec{n})$ depend *linearly* on $\{|c_{\alpha}|^2\}$, but the associated linear map has a nontrivial kernel. As a result, deriving an analog of Eq. (23) requires a partial inversion of this map, a strategy first employed in the fermionic context in Ref. [22]. We now adapt this approach to the bosonic setting and refine it.

To this end, we fix an occupation number vector \vec{n} in the domain and let $|\Psi\rangle = \sum_{\alpha} c_{\alpha} |\vec{n}^{(\alpha)}\rangle$ be an N -particle state in $\mathcal{H}_N^{(P)}$ with momentum occupation numbers \vec{n} .

Using Eq. (17), we obtain

$$\begin{aligned}
D^{(j)}(\vec{n}) &= \vec{\kappa}^{(j)} \cdot \vec{n} + \mu^{(j)} \\
&= \langle \Psi | \sum_{k=0}^{d-1} \kappa_k^{(j)} \hat{n}_k + \mu^{(j)} | \Psi \rangle \\
&= \sum_{\alpha} |c_{\alpha}|^2 [\vec{\kappa}^{(j)} \cdot \vec{n}^{(\alpha)} + \mu^{(j)}] \\
&= \sum_{\alpha} |c_{\alpha}|^2 D^{(j)}(\vec{n}^{(\alpha)}),
\end{aligned} \tag{27}$$

where $\hat{n}_k \equiv \hat{b}_k^\dagger \hat{b}_k$. Introducing the vector \vec{y} with components $y_{\alpha} \equiv |c_{\alpha}|^2 \geq 0$ and the matrix $T \in \mathbb{R}^{J \times \dim \mathcal{H}_N^{(P)}}$ defined by $T_{j\alpha} \equiv D^{(j)}(\vec{n}^{(\alpha)}) \geq 0$, this relation can be written compactly as

$$\vec{D}(\vec{n}) = T \vec{y}. \tag{28}$$

At this point, \vec{n} (and hence $\vec{D}(\vec{n})$) is given, and the task is to determine all nonnegative vectors \vec{y} solving Eq. (28).

A natural tool to address this problem is the *Moore-Penrose pseudoinverse*. For a real matrix T with singular value decomposition $T = U \Sigma V^\top$, the pseudoinverse is defined as $T^+ = V \Sigma^+ U^\top$, where Σ^+ is obtained from Σ by

inverting the nonzero diagonal elements (the singular values) of Σ and transposing. The pseudoinverse provides a canonical (least-norm) solution to underdetermined linear systems and, crucially, allows one to separate the uniquely determined components from contributions lying in the kernel of T .

Applying this construction to Eq. (28), the general solution can be written as

$$\vec{y} = T^+ \vec{D}(\vec{n}) + \vec{x}, \tag{29}$$

where \vec{x} is an arbitrary vector in the kernel of T and must be chosen such that the resulting \vec{y} has nonnegative components. To verify that Eq. (29) indeed solves Eq. (28), note that by N -representability of \vec{n} there exists a vector \vec{y}' with $\vec{D}(\vec{n}) = T \vec{y}'$, and the defining property $TT^+T = T$ of the Moore-Penrose pseudoinverse then implies $T\vec{y} = \vec{D}(\vec{n})$.

We may therefore write

$$|\Psi\rangle = \sum_{\alpha=1}^{\dim \mathcal{H}_N^{(P)}} \eta_{\alpha} \sqrt{\sum_{j=1}^J T_{\alpha j}^+ D^{(j)}(\vec{n}) + x_{\alpha} |\vec{n}^{(\alpha)}\rangle}, \tag{30}$$

where the phases $\{\eta_{\alpha}\}$ are at this stage free. Inserting this expression into the constrained-search formulation (12) yields

$$\mathcal{F}[\vec{n}] = \sum_{\alpha, \beta=1}^{\dim \mathcal{H}_N^{(P)}} W_{\alpha \beta} \eta_{\alpha}^* \eta_{\beta} \sqrt{\sum_{j=1}^J T_{\alpha j}^+ D^{(j)}(\vec{n}) + x_{\alpha}} \sqrt{\sum_{j=1}^J T_{\beta j}^+ D^{(j)}(\vec{n}) + x_{\beta}}. \tag{31}$$

For each \vec{n} in the domain, the phases η_{α} and the vector $\vec{x} \in \ker(T)$ are chosen so as to minimize Eq. (31). If, in addition to translational invariance, the Hamiltonian is invariant under parity-time (PT) symmetry, the phases can be taken real without changing the resulting ground-state energy, yielding an equivalent functional [19].

Equation (31) reveals a deep connection between the universal interaction functional \mathcal{F} and the geometry of its domain. In this representation, all nontrivial dependence on the occupation numbers enters through the facet-distance coordinates $\vec{D}(\vec{n})$, which are naturally adapted to the shape of the admissible set. Apart from the minimizing choice of the kernel vector \vec{x} , the general form of the functional is therefore largely dictated by the geometry of the domain rather than by the specific interaction \hat{W} . Viewed in this way, Eq. (31) constitutes a geometry-driven reparametrization of the constrained-search functional, suggesting a shift in how constrained-search approaches may be formulated more broadly.

We now illustrate this general construction by means of an explicit example, which also demonstrates how the formalism reproduces the simplex result as a special case.

For $d = 2$, $N = 4$, and $P = 0$, the domain of \mathcal{F} is given by the convex hull of $\vec{n}^{(1)} = (4, 0)$, $\vec{n}^{(2)} = (2, 2)$, and $\vec{n}^{(3)} = (0, 4)$ (see panel (a) of Fig. 3). The domain is one-dimensional and has two facets, corresponding to the vertices $\vec{n}^{(1)}$ and $\vec{n}^{(3)}$, which give rise to the constraints $D^{(1)}(\vec{n}) = n_0 \geq 0$ and $D^{(2)}(\vec{n}) = n_1 \geq 0$. The resulting matrix $T = (D^{(j)}(\vec{n}^{(\alpha)}))$ reads

$$T = \begin{pmatrix} 4 & 2 & 0 \\ 0 & 2 & 4 \end{pmatrix}. \tag{32}$$

Its singular value decomposition is

$$T = \begin{pmatrix} -\frac{1}{\sqrt{2}} & \frac{1}{\sqrt{2}} \\ \frac{1}{\sqrt{2}} & \frac{1}{\sqrt{2}} \end{pmatrix} \begin{pmatrix} 4 & 0 & 0 \\ 0 & 2\sqrt{6} & 0 \end{pmatrix} \begin{pmatrix} -\frac{1}{\sqrt{2}} & \frac{1}{\sqrt{3}} & -\frac{1}{\sqrt{6}} \\ 0 & \frac{1}{\sqrt{3}} & \frac{1}{\sqrt{6}} \\ \frac{1}{\sqrt{2}} & \frac{1}{\sqrt{3}} & -\frac{1}{\sqrt{6}} \end{pmatrix}^\top, \tag{33}$$

from which the pseudoinverse follows as

$$\begin{aligned} T^+ &= \begin{pmatrix} -\frac{1}{\sqrt{2}} & \frac{1}{\sqrt{3}} & -\frac{1}{\sqrt{6}} \\ 0 & \frac{1}{\sqrt{3}} & \frac{2}{\sqrt{6}} \\ \frac{1}{\sqrt{2}} & \frac{1}{\sqrt{3}} & -\frac{1}{\sqrt{6}} \end{pmatrix} \begin{pmatrix} \frac{1}{4} & 0 & 0 \\ 0 & \frac{1}{2\sqrt{6}} & 0 \end{pmatrix}^\top \begin{pmatrix} -\frac{1}{\sqrt{2}} & \frac{1}{\sqrt{2}} \\ \frac{1}{\sqrt{2}} & \frac{1}{\sqrt{2}} \end{pmatrix}^\top \\ &= \frac{1}{24} \begin{pmatrix} 5 & -1 \\ 2 & 2 \\ -1 & 5 \end{pmatrix}. \end{aligned} \quad (34)$$

The kernel of T is spanned by $(-1, 2, -1)$, so that $\vec{x} = \xi(-1, 2, -1)$. The radicands in Eq. (31) are then given by

$$\begin{aligned} T^+ \vec{D}(\vec{n}) + \vec{x} &= \frac{1}{24} \begin{pmatrix} 5 & -1 \\ 2 & 2 \\ -1 & 5 \end{pmatrix} \begin{pmatrix} n_0 \\ n_1 \end{pmatrix} + \xi \begin{pmatrix} -1 \\ 2 \\ -1 \end{pmatrix} \\ &= \begin{pmatrix} \frac{1}{3} + \frac{1}{8}(n_1 - n_2) - \xi \\ \frac{1}{3} + 2\xi \\ \frac{1}{3} - \frac{1}{8}(n_1 - n_2) - \xi \end{pmatrix}. \end{aligned} \quad (35)$$

Assuming $W_{13} = 0$, $W_{11} = W_{33}$, and $W_{12} = W_{23} \equiv w$, as is the case for the Bose-Hubbard model, Eq. (15), and setting $W_{11} = W_{33} = 0$ without loss of generality, a minimizing choice of phases is $(\eta_1, \eta_2, \eta_3) = (1, -1, 1)$. Equation (31) then yields

$$\begin{aligned} \mathcal{F}[\vec{n}] &= W_{22} \left(\frac{1}{3} + 2\xi \right) - 2|w| \sqrt{\frac{1}{3} + 2\xi} \times \\ &\quad \left[\sqrt{\frac{1}{3} + \frac{1}{8}(n_1 - n_2) - \xi} + \sqrt{\frac{1}{3} - \frac{1}{8}(n_1 - n_2) - \xi} \right]. \end{aligned} \quad (36)$$

We emphasize that Eq. (31) provides an *exact* representation of the functional \mathcal{F} . While its explicit evaluation remains challenging for general interactions \hat{W} , due to the dependence of \vec{x} and the phases η_α on \vec{n} and the typically large nullity of T , the formalism makes explicit how the geometry of the domain constrains the functional form. In this way, it naturally suggests systematic approximation strategies based on controlled estimates of the kernel contribution $\vec{x}[\vec{n}]$, an idea we will pursue further in Sec. VI.

V. GENERALIZED BEC FORCE

A central theme of this work has been to elucidate how the geometry of the domain of the universal functional \mathcal{F} controls both its structure and its physical implications. In the preceding sections, we established that the functional admits an explicit representation in terms of distances $D^{(j)}$ of \vec{n} to the facets of its domain and that these distances encode nontrivial many-body information. In this section, we demonstrate that this geometric perspective has direct and quantitative consequences for the *variational behavior* of the functional: specifically, it

gives rise to a repulsive force whenever the natural occupation number vector \vec{n} approaches the boundary of $\text{dom}(\mathcal{F})$.

We begin by observing, based on Eq. (23), that within the simplex setting the functional takes the approximate form $\mathcal{F}[\vec{n}] \sim c_0 - c_1 \sqrt{D^{(\omega)}(\vec{n})}$ whenever the distance $D^{(\omega)}(\vec{n})$ to a facet approaches zero. As a direct consequence, the gradient of the functional diverges according to $\nabla_{\vec{n}} \mathcal{F} \sim 1/\sqrt{D^{(\omega)}(\vec{n})}$ as $D^{(\omega)} \rightarrow 0$. This already suggests that the boundary of the domain is dynamically inaccessible for ground states, since the functional develops an infinite slope that repels the ground-state occupation number vector \vec{n} back into the interior of the domain.

To substantiate and generalize this observation, we now investigate the behavior of the gradient $\nabla_{\vec{n}} \mathcal{F}$ numerically for the one-dimensional Bose-Hubbard model with $d = 3$, for which the domain of admissible natural occupation numbers is two-dimensional. For several particle numbers N and total momenta P , we evaluate the magnitude $|\nabla_{\vec{n}} \mathcal{F}|$ throughout the domain and visualize the result in Fig. 5. Our numerical procedure exploits the relation

$$\nabla_{\vec{n}} \mathcal{F}(\vec{n}) = -\vec{t}, \quad (37)$$

which holds whenever \vec{n} corresponds to a ground state of the Hamiltonian $\hat{t} + \hat{W}$ for some kinetic energy operator $\hat{t} = \sum_k t_k \hat{n}_k$. By scanning over a sufficiently large set of kinetic energy vectors \vec{t} , we obtain the exact value of the pure-state functional (12) for all occupation number vectors \vec{n} that arise from ground states (often referred to as v -representable, or, in the present context, t -representable). Points \vec{n} that do not correspond to ground states of any such \hat{t} are shown in black in Fig. 5. Since these points typically do not lie close to the boundary of $\text{dom}(\mathcal{F})$, the resulting data are fully sufficient for resolving the behavior of the functional gradient in the boundary regime relevant for our purposes.

Inspection of Fig. 5 reveals a clear and robust pattern: in all cases considered, the gradient of the functional diverges as the boundary of the domain is approached. This divergence is neither confined to particular facets nor to specific values of (N, P) , but instead appears as a generic feature of the functional.

Divergences of this type have recently been observed in a variety of reduced density matrix functional settings. When the quantity playing the role of the basic variable of the functional theory approaches the boundary of the functional's domain, the corresponding derivative typically diverges as the inverse square root of the distance to that boundary [22, 24, 28, 98]. In fermionic systems, this behavior, referred to as the *exchange force*, has been demonstrated explicitly for translationally invariant one-band lattice models as well as for the asymmetric lattice dimer model with generic pair interaction [22]. For bosonic systems, the analogous divergence has so far been established only in the vicinity of a specific boundary point of the domain, namely the Bose-Einstein

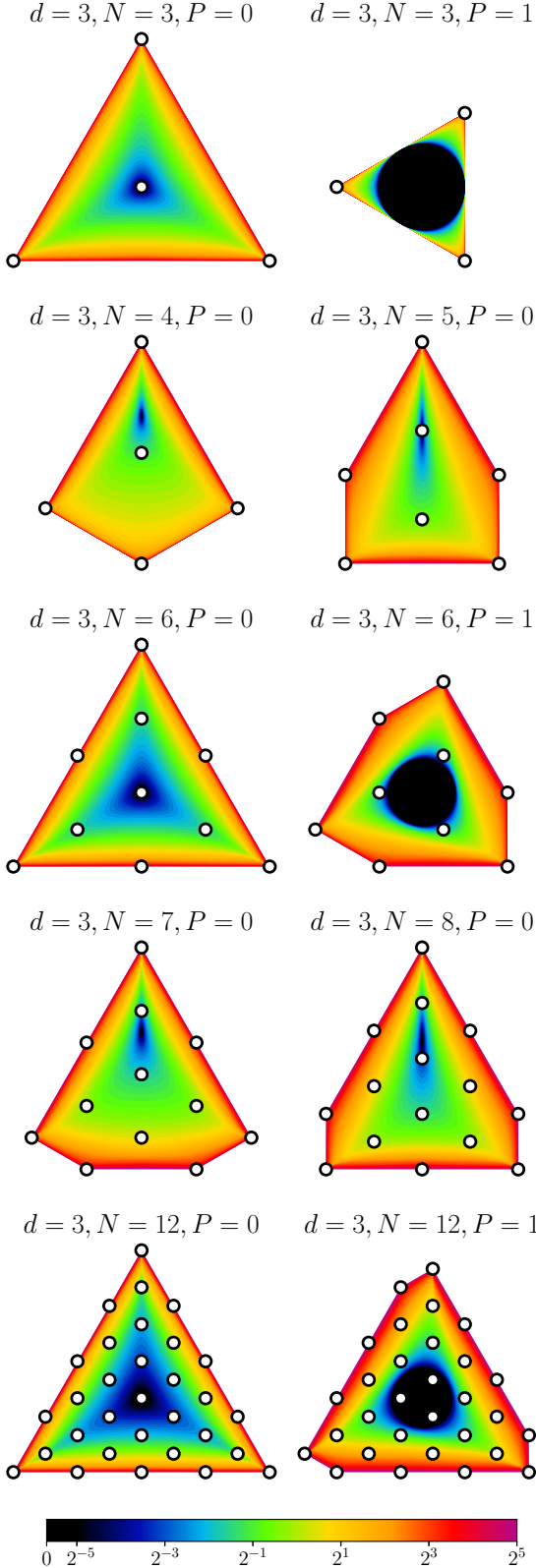


FIG. 5. Magnitude of the gradient $|\nabla_{\vec{n}} \mathcal{F}|$ for $d = 3$ and various combinations of (N, P) . See text for more details.

condensate vertex $(N, 0, \dots)$, where it is known as the *BEC force* [24, 28, 98].

A key result of this section is that such a force is not confined to the vicinity of the BEC vertex. Rather, it arises generically near *any* facet of the domain $\text{dom}(\mathcal{F})$. For this reason, we refer to it as the *generalized BEC force*. Its presence has important consequences, most notably the prohibition of *pinning*, i.e., situations in which the ground-state occupation number vector lies exactly on the boundary of the set of pure (N, P) -representable \vec{n} [76, 99–101]. This result is closely related to the question of whether natural occupation numbers of the ground state can vanish, since any such vanishing would necessarily place \vec{n} on the boundary of the domain [102].

In the following, we go beyond merely establishing the presence of a diverging force at the boundary of the functional domain. We provide a direct and general proof of this divergence and, for the first time, derive a simple closed expression for its prefactor. This quantity determines the strength of the generalized BEC force and constitutes a central result of this work. It yields a sharp criterion for the presence or absence of pinning and establishes an exact constraint that the functional of *any* translation-invariant bosonic system must satisfy, independently of the interaction \hat{W} . More broadly, our derivation demonstrates that repulsive boundary forces are a generic and structural feature of functional theories.

Before proceeding, we fix a convention. As noted after Eq. (19) in Sec. IV, the facet-defining coefficients $\vec{\kappa}^{(j)}$ and $\mu^{(j)}$ are not unique. Throughout this section, we choose their normalization such that $\vec{\kappa}^{(j)}$ is tangent to the domain of \mathcal{F} and satisfies $\vec{\kappa}^{(j)} \cdot \vec{\kappa}^{(j)} = 1$. In most cases, tangentiality is equivalent to imposing $\sum_{\alpha} \kappa_{\alpha}^{(j)} = 0$. For example, the first constraint in Eq. (20) for $(d, N, P) = (3, 3, 1)$ becomes

$$D^{(1)}(\vec{n}) = \frac{n_0 - n_2 + 1}{\sqrt{2}}, \quad (38)$$

for which $\vec{\kappa}^{(1)} = \frac{1}{\sqrt{2}}(1, 0, -1)$ and $\mu^{(1)} = \frac{1}{\sqrt{2}}$. This choice is purely conventional and serves to simplify the expressions that follow.

A. The Simplex

As in Sec. IV A, additional insight can be gained by first analyzing the problem under the assumption that $\text{dom}(\mathcal{F})$ is a simplex with $\dim \mathcal{H}_N^{(P)}$ vertices. While a heuristic argument for a diverging repulsive force in the simplex setting was already given at the beginning of this section, we now derive an explicit expression for the repulsion strength \mathcal{G} (defined in Eq. (39)). Recall (see Sec. IV A) that the occupation number vectors $\vec{n}^{(\alpha)}$, $\alpha = 1, \dots, \dim \mathcal{H}_N^{(P)}$, are associated with constraints $D^{(\alpha)}(\vec{n}) \geq 0$ corresponding to the facets opposite to $\vec{n}^{(\alpha)}$. Pick an arbitrary facet $1 \leq \omega \leq \dim \mathcal{H}_N^{(P)}$, i.e.,

the one opposite the vertex $\vec{n}^{(\omega)}$, and consider the behavior of \mathcal{F} in a small neighborhood of a point \vec{n}^* on this facet. By construction, $D^{(\omega)}(\vec{n}^*) = 0$, and we investigate $\mathcal{F}[\vec{n}^* + \epsilon \vec{v}]$ for some inward-pointing vector \vec{v} . For simplicity, we assume that \vec{n}^* does not lie on any other facet, i.e., $D^{(\alpha)}(\vec{n}^*) > 0$ for all $\alpha \neq \omega$.

In principle, the analysis could be carried out for an arbitrary inward-pointing direction \vec{v} . However, the result would not differ qualitatively: if a generalized BEC force exists, then displacements tangential to the facet induce only subleading variations of \mathcal{F} . Accordingly, we choose $\vec{v} = \vec{\kappa}^{(\omega)}$, where $\vec{\kappa}^{(\omega)}$ denotes the vector of coefficients of the linear part of the constraint $D^{(\omega)}$, as defined in Eq. (19). By construction, $\vec{\kappa}^{(\omega)}$ is the inward-pointing unit vector normal to the facet ω .

We now employ Eq. (23) to analyze $\mathcal{F}[\vec{n}^* + \epsilon \vec{\kappa}^{(\omega)}]$. More precisely, we compute the derivative

$$\mathcal{G}[\vec{n}^*] \equiv \frac{d}{d\sqrt{\epsilon}} \Big|_{\epsilon=0} \mathcal{F}[\vec{n}^* + \epsilon \vec{\kappa}^{(\omega)}], \quad (39)$$

which we refer to as the *repulsion strength* of the generalized BEC force at \vec{n}^* . If one were to compute $d\mathcal{F}/d\epsilon$ at $\vec{n}^* + \epsilon \vec{\kappa}^{(\omega)}$ instead, the leading contribution would scale as $\frac{1}{2\sqrt{\epsilon}} \mathcal{G}[\vec{n}^*]$, up to terms that are subleading in the limit $\epsilon \rightarrow 0$. Hence, $\mathcal{G}[\vec{n}^*]$ corresponds, up to a factor of 2, to the prefactor of the diverging $1/\sqrt{\epsilon}$ repulsive force.

A straightforward calculation yields

$$D^{(\alpha)}(\vec{n}^* + \epsilon \vec{\kappa}^{(\omega)}) = D^{(\alpha)}(\vec{n}^*) + \epsilon \vec{\kappa}^{(\alpha)} \cdot \vec{\kappa}^{(\omega)}, \quad (40)$$

which for $\alpha = \omega$ reduces to

$$D^{(\omega)}(\vec{n}^* + \epsilon \vec{\kappa}^{(\omega)}) = \epsilon. \quad (41)$$

While Eq. (41) is expected, ϵ parameterizes the distance to \vec{n}^* , and $D^{(\omega)}$ measures the distance to the facet; it also confirms that $\vec{\kappa}^{(\omega)}$ indeed points inward, as assumed. Substituting Eq. (41) into Eq. (23), separating the terms involving ω , and performing the minimization over the phase η_ω , we obtain

$$\begin{aligned} \mathcal{F}[\vec{n}^* + \epsilon \vec{\kappa}^{(\omega)}] = \min_{\{\eta_{\alpha \neq \omega}\}} & \left[\sum_{\substack{\alpha \neq \omega \\ \beta \neq \omega}} \eta_\alpha^* \eta_\beta W_{\alpha\beta} \sqrt{\frac{D^{(\alpha)}(\vec{n}^* + \epsilon \vec{\kappa}^{(\omega)})}{L_\alpha}} \sqrt{\frac{D^{(\beta)}(\vec{n}^* + \epsilon \vec{\kappa}^{(\omega)})}{L_\beta}} \right. \\ & \left. - 2 \sqrt{\frac{\epsilon}{L_\omega}} \left| \sum_{\alpha \neq \omega} \eta_\alpha W_{\omega\alpha} \sqrt{\frac{D^{(\alpha)}(\vec{n}^* + \epsilon \vec{\kappa}^{(\omega)})}{L_\alpha}} \right| + \frac{\epsilon}{L_\omega} W_{\omega\omega} \right]. \end{aligned} \quad (42)$$

Our objective is to evaluate the derivative with respect to $\sqrt{\epsilon}$ at $\epsilon = 0$ (Eq. (39)). This can be achieved using Danskins theorem [103], which allows the interchange of minimization and differentiation for directional derivatives. This is sufficient for the present analysis, even though it does not necessarily imply differentiability of the functional \mathcal{F} . The minimization must, however, be restricted to the set of minimizers of the original problem. One thus finds

$$\mathcal{G}[\vec{n}^*] = -\frac{2}{\sqrt{L_\omega}} \widetilde{\min}_{\{\eta_{\alpha \neq \omega}\}} \left| \sum_{\alpha \neq \omega} \eta_\alpha W_{\omega\alpha} \sqrt{\frac{D^{(\alpha)}(\vec{n}^*)}{L_\alpha}} \right|, \quad (43)$$

where $\widetilde{\min}$ indicates that the phases $\{\eta_{\alpha \neq \omega}\}$ are restricted to those minimizing Eq. (42). Introducing the state $|\Phi^*(\vec{n}^*)\rangle = \sum_{\alpha \neq \omega} \eta_\alpha \sqrt{D^{(\alpha)}(\vec{n}^*)/L_\alpha} |\vec{n}^{(\alpha)}\rangle$, which is precisely the wave function minimizing the constrained search (12) at \vec{n}^* , we may write

$$\mathcal{G}[\vec{n}^*] = -2 \frac{|\langle \vec{n}^{(\omega)} | \hat{W} | \Phi^*(\vec{n}^*) \rangle|}{\sqrt{L_\omega}}. \quad (44)$$

The minus sign reflects the repulsive nature of the force since $\mathcal{G} = d\mathcal{F}/d\sqrt{\epsilon}$ and increasing ϵ corresponds to moving away from the facet. The geometric factor $\sqrt{L_\omega}$ in

the denominator implies that the repulsion weakens as the distance between the vertex $\vec{n}^{(\omega)}$ and the facet increases. Physically, this expresses that the state $|\vec{n}^{(\omega)}\rangle$ becomes less relevant for describing densities near the facet, since any finite overlap with this state requires deviations from the facet that scale with $L_\omega = D^{(\omega)}(\vec{n}^{(\omega)})$. This also motivates our normalization $|\vec{\kappa}^{(\omega)}|^2 = 1$, ensuring that $D^{(\omega)}(\vec{n})$ coincides with the actual distance to the facet.

B. Beyond the simplex

We now drop the simplex assumption and derive a general expression for the repulsion strength \mathcal{G} for arbitrary settings (d, N, P) . As is often the case, abandoning the simplex structure introduces substantial complications. Most importantly, there is no longer a one-to-one correspondence between facets of $\text{dom}(\mathcal{F})$ and occupation number vectors $\{\vec{n}^{(\alpha)}\}$. Instead, the domain is characterized by J constraints $D^{(j)} \geq 0$, $j = 1, \dots, J$, where J is now smaller than the number of configuration states $\dim \mathcal{H}_N^{(P)}$. To avoid confusion, we therefore use Latin indices j, s, \dots to label facets and Greek indices α, ω, \dots to label configuration states.

Proceeding analogously to the simplex case, and as it

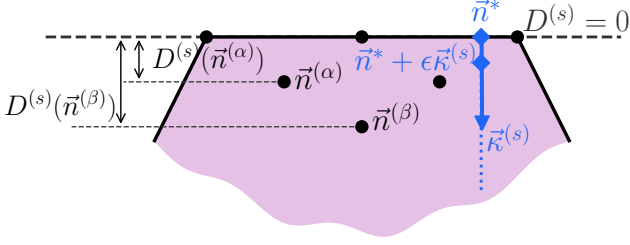


FIG. 6. Geometric setup underlying the derivation of the generalized BEC force. Shown are a facet $D^{(s)}(\vec{n}) = 0$, its inward normal $\vec{\kappa}^{(s)}$, and the normal path $\vec{n}^* + \epsilon \vec{\kappa}^{(s)}$ used in the analysis. See the main text for details.

is illustrated in Fig. 6, we fix a facet $1 \leq s \leq J$ and a point \vec{n}^* on it, such that $D^{(s)}(\vec{n}^*) = 0$. We assume that \vec{n}^* does not lie on any other facet, i.e., $D^{(j)}(\vec{n}^*) > 0$ for all $j \neq s$. Mimicking the definition of the repulsion strength in the simplex setting [Eq. (39)], we define

$$\mathcal{G}[\vec{n}^*] \equiv \frac{d}{d\sqrt{\epsilon}} \Big|_{\epsilon=0} \mathcal{F}[\vec{n}^* + \epsilon \vec{\kappa}^{(s)}]. \quad (45)$$

After a sequence of rather technical and involved steps, which are presented in Appendix A, one arrives at

$$\mathcal{G}[\vec{n}^*] = -2 \left[\sum_{\alpha: D^{(s)}(\vec{n}^{(\alpha)}) > 0} \frac{\left| \langle \vec{n}^{(\alpha)} | \hat{W} | \Phi^*(\vec{n}^*) \rangle \right|^2}{D^{(s)}(\vec{n}^{(\alpha)})} \right]^{1/2}, \quad (46)$$

where $|\Phi^*(\vec{n}^*)\rangle$ denotes a minimizer of the constrained search [Eq. (12)] at \vec{n}^* . If multiple minimizers exist, $|\Phi^*(\vec{n}^*)\rangle$ is chosen such that the expression in Eq. (46) is minimized.

Equation (46) constitutes the central result of this section. Together with the definition (45), it implies that the gradient $\nabla_{\vec{n}} \mathcal{F}$ diverges as $1/\sqrt{\epsilon}$ as \vec{n} approaches a facet at distance $\epsilon \rightarrow 0$, provided that the sum in Eq. (46) does not vanish. Several notable features of this result deserve emphasis. First, the overall minus sign reflects the repulsive nature of the force, in agreement with the simplex analysis in Sec. V A. Second, each configuration state $|\vec{n}^{(\alpha)}\rangle$ contributes with a geometric weight $D^{(s)}(\vec{n}^{(\alpha)})^{-1}$ (see Fig. 6), i.e., inversely proportional to its distance from the facet. Consequently, configuration states far from the facet have a suppressed influence on the repulsion strength. Third, since the radicand is a sum of non-negative terms, the repulsion strength can vanish only if $\langle \vec{n}^{(\alpha)} | \hat{W} | \Phi^*(\vec{n}^*) \rangle = 0$ for all α satisfying $D^{(s)}(\vec{n}^{(\alpha)}) > 0$.

Finally, it is instructive to recover the simplex result from Eq. (46). In the simplex setting, there is exactly one configuration state $|\vec{n}^{(\alpha)}\rangle$ not lying on the facet, so the sum reduces to a single term and Eq. (46) reproduces Eq. (43). The explicit appearance of the factor $D^{(s)}(\vec{n}^{(\alpha)})^{-1}$ thus confirms, in full generality, the geometric intuition developed in the simplex case.

We now illustrate Eq. (46) by considering the one-dimensional Bose-Hubbard model with $(d, N, P) = (3, N, 0)$, where N is a multiple of 3. The cases $N = 6$ and $N = 12$ are shown in the third and fifth rows of the left column of Fig. 5, respectively. Although the domain is a 2-simplex (a triangle), this situation does not fall into what we termed the ‘simplex setting’, since additional occupation number vectors exist beyond the vertices $(N, 0, 0)$, $(0, N, 0)$, and $(0, 0, N)$.

We choose s to label the facet corresponding to the lower edge of the simplex, for which

$$D^{(s)}(\vec{n}) = \frac{1}{\sqrt{6}}(2n_0 - n_1 - n_2) + \frac{N}{\sqrt{6}}, \quad (47)$$

so that $\vec{\kappa}^{(s)} = \frac{1}{\sqrt{6}}(2, -1, -1)$ and $\mu^{(s)} = N/\sqrt{6}$. Points on this facet may be parameterized as $\vec{n}^* = (0, N\lambda, N(1-\lambda))$ with $\lambda \in (0, 1)$, for which $D^{(s)}(\vec{n}^*) = 0$ holds identically.

To apply Eq. (46), we first note that the configuration states lying on the facet are

$$|0, N, 0\rangle, |0, N-3, 3\rangle, \dots, |0, 0, N\rangle. \quad (48)$$

The minimizers of the constrained search at \vec{n}^* are given by

$$|\Phi^*(\theta)\rangle = \sqrt{\lambda} |0, N, 0\rangle + \sqrt{1-\lambda} e^{i\theta} |0, 0, N\rangle. \quad (49)$$

This follows from two facts: first, the interaction \hat{W} does not couple states lying on the facet (a property of any two-body interaction), and second, among all facet states, $|0, N, 0\rangle$ and $|0, 0, N\rangle$ have the lowest interaction energy, which is specific to the Bose-Hubbard model.

The states $|0, N, 0\rangle$ and $|0, 0, N\rangle$ couple only to $|1, N-2, 1\rangle$ and $|1, 1, N-2\rangle$, respectively, with matrix elements $\langle 1, N-2, 1 | \hat{W} | 0, N, 0 \rangle = \langle 1, 1, N-2 | \hat{W} | 0, 0, N \rangle = \frac{2}{3}\sqrt{N(N-1)}$. Both off-facet states lie at the same distance from the facet, $D^{(s)}(1, N-2, 1) = D^{(s)}(1, 1, N-2) = \sqrt{6}/2$. Substituting these ingredients into Eq. (46) yields

$$\begin{aligned} \mathcal{G}[0, \lambda N, (1-\lambda)N] &= -2 \left[\frac{\left(\frac{2}{3}\sqrt{N(N-1)} \right)^2 (\lambda + (1-\lambda))}{\frac{\sqrt{6}}{2}} \right]^{1/2} \\ &= -\frac{4 \cdot 2^{1/4} \cdot 3^{3/4}}{9} \sqrt{N(N-1)}. \end{aligned} \quad (50)$$

This analysis applies for $N \geq 6$; for $N = 3$, the states $|1, N-2, 1\rangle$ and $|1, 1, N-2\rangle$ coincide. Numerically, the prefactor is approximately 1.205. Notably, the resulting repulsion strength $\mathcal{G}[\vec{n}^*]$ is independent of the position λ along the facet.

To verify that Eq. (50) indeed yields the correct repulsion strength, we approximate the functional as

$$\mathcal{F}[\vec{n}^* + \epsilon \vec{\kappa}^{(s)}] \approx \mathcal{F}[\vec{n}^*] + \sqrt{\epsilon} \mathcal{G}[\vec{n}^*], \quad (51)$$

and compare this approximation with numerical results. Choosing $\vec{n}^* = (0, N/2, N/2)$, for which $\mathcal{F}[\vec{n}^*] = N(N -$

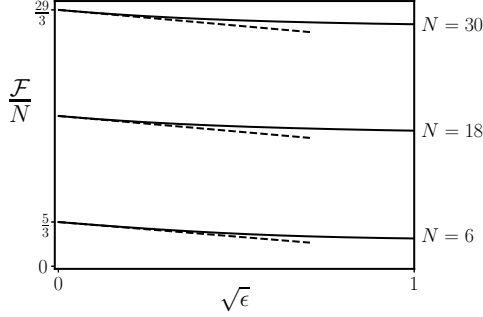


FIG. 7. Comparison of the approximation (52) (dashed lines) with exact numerical results (solid lines) for the universal functional in the Bose-Hubbard model (15) for $(d, N, P) = (3, N, 0)$.

$1)/3$, we obtain

$$\frac{\mathcal{F}[\vec{n}^* + \epsilon \vec{\kappa}^{(s)}]}{N} \approx \frac{N-1}{3} - 1.205 \sqrt{\epsilon} \sqrt{\frac{N-1}{N}}. \quad (52)$$

Figure 7 compares this expression to the exact functional for $N = 6, 18, 30$. The agreement of the slopes at $\epsilon = 0$ demonstrates that Eq. (50) provides the correct repulsion strength at \vec{n}^* .

Finally, we remark that Eq. (46) also explains the larger generalized BEC force observed for $P = 1$ compared to $P = 0$ at fixed $(d = 3, N)$ when N is a multiple of 3 (see Fig. 5). For $P = 1$, minimizing states on a facet still involve only the two extremal states (cf. Fig. 8), but these now couple to five off-facet states, rather than two as in the $P = 0$ case. Consequently, the sum in Eq. (46) contains five terms instead of two, leading to a larger repulsion strength. This mechanism is illustrated in Fig. 8 for $N = 12$.

To summarize this section, Eq. (46) provides an explicit and universal characterization of the leading boundary singularity of \mathcal{F} , separating geometric information encoded in the facet distances $D^{(s)}(\vec{n}^{(\alpha)})$ from interaction effects entering through the matrix elements $\langle \vec{n}^{(\alpha)} | \hat{W} | \Phi^*(\vec{n}^*) \rangle$. The resulting square-root divergence of $\nabla_{\vec{n}} \mathcal{F}$ is therefore not a model-dependent artifact but a direct consequence of the constrained-search structure near facets of $\text{dom}(\mathcal{F})$. This perspective suggests a concrete route for constructing approximate functionals that enforce the correct near-facet behavior by design, while retaining flexibility in modeling the physically relevant interaction contributions.

VI. PROOF OF CONCEPT: A COMPLETE ILLUSTRATIVE EXAMPLE

In this section we present a self-contained, concrete analysis that illustrates all essential ingredients developed in Secs. III–V. Beyond serving as an explicit validation of our general framework, the example is designed

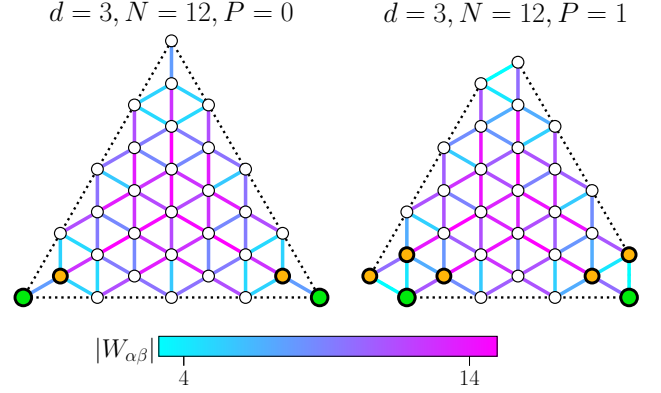


FIG. 8. Graphical explanation of the stronger generalized BEC force for $P = 1$. Two occupation number vectors $\vec{n}^{(\alpha)}, \vec{n}^{(\beta)}$ are connected if $W_{\alpha\beta} \neq 0$, with color encoding of the coupling $|W_{\alpha\beta}|$ between their configuration states $|\vec{n}^{(\alpha)}\rangle, |\vec{n}^{(\beta)}\rangle$. On a given facet, the extremal states (green) couple to two off-facet states (orange) for $P = 0$ and to five off-facet states for $P = 1$. See text for details.

to demonstrate its practical relevance: it yields a compact representation of the exact functional and provides a transparent route to accurate, physics-informed functional approximations.

We consider the one-dimensional Bose-Hubbard model with $N = 3$ bosons on $d = 3$ lattice sites and restrict to the total momentum sector $P = 0$. For this system, the functional \mathcal{F} can in principle be obtained in closed form, because it follows from the ground-state energies of the Hamiltonian $\hat{H}(\hat{t}) = \hat{t} + \hat{W}$ that takes the form of a 4×4 matrix. However, the resulting quartic expressions are cumbersome and offer little insight. Instead, we proceed in a way that mirrors the general strategy of this work and, crucially, produces an approximation for \mathcal{F} that is both simple and highly accurate when benchmarked against numerical calculations.

For clarity, we organize the discussion and derivation into three steps:

- (1) Identify the symmetry sector $\mathcal{H}_N^{(P)}$ and determine the vertices spanning the domain $\text{dom}(\mathcal{F})$.
- (2) Convert $\text{dom}(\mathcal{F})$ to a hyperplane (facet) representation; compute the matrix T (28) and its kernel.
- (3) Apply Eq. (31) and construct a controlled approximation, highlighting the role of the generalized BEC force.

The approximation and its numerical validation are presented in Sec. VIC.

A. Identifying the symmetry sector and the domain of the functional

The total N -particle Hilbert space \mathcal{H}_N is spanned by the ten configuration states $|3, 0, 0\rangle, |2, 1, 0\rangle, \dots, |0, 0, 3\rangle$.

The $P = 0$ symmetry sector $\mathcal{H}_N^{(0)}$ is a four-dimensional subspace spanned by

$$\begin{aligned} |\vec{n}^{(1)}\rangle &\equiv |3,0,0\rangle, & |\vec{n}^{(2)}\rangle &\equiv |0,3,0\rangle, & |\vec{n}^{(3)}\rangle &\equiv |0,0,3\rangle, \\ |\vec{n}^{(4)}\rangle &\equiv |1,1,1\rangle. \end{aligned} \quad (53)$$

Their occupation number vectors $\vec{n}^{(\alpha)}$, $\alpha = 1, \dots, 4$, then span the domain of the universal functional $\mathcal{F}^{(0)}$ (see panel (c) of Fig. 3). Restricted to $\mathcal{H}_3^{(0)}$ and expressed in this basis, the Bose-Hubbard interaction operator \hat{W} (Eq. (15)) takes the form

$$\hat{W} = \begin{pmatrix} 2 & 0 & 0 & \frac{2\sqrt{6}}{3} \\ 0 & 2 & 0 & \frac{2\sqrt{6}}{3} \\ 0 & 0 & 2 & \frac{2\sqrt{6}}{3} \\ \frac{2\sqrt{6}}{3} & \frac{2\sqrt{6}}{3} & \frac{2\sqrt{6}}{3} & 4 \end{pmatrix}. \quad (54)$$

This explicit reduction already captures the first central theme of our work: symmetries substantially simplify the structure of \mathcal{F} by reducing both the relevant Hilbert space and the geometry of the functional domain.

B. Hyperplane (facet) representation and finding the kernel of T

Following Sec. IV B, we compute the facet constraints $D^{(j)}$ and the matrix T that encodes the distances of the vertices to the facets. Since $\text{dom}(\mathcal{F})$ is a 2-simplex (panel (c) of Fig. 3), there are three facets and hence three constraints:

$$\begin{aligned} D^{(1)}(\vec{n}) &\equiv \frac{1}{\sqrt{6}}(2n_0 - n_1 - n_2) + \frac{3}{\sqrt{6}} \geq 0 \\ D^{(2)}(\vec{n}) &\equiv \frac{1}{\sqrt{6}}(2n_1 - n_0 - n_2) + \frac{3}{\sqrt{6}} \geq 0 \\ D^{(3)}(\vec{n}) &\equiv \frac{1}{\sqrt{6}}(2n_2 - n_0 - n_1) + \frac{3}{\sqrt{6}} \geq 0, \end{aligned} \quad (55)$$

where the coefficients are chosen such that $|\vec{\kappa}^{(j)}| = 1$ and $\sum_{k=0}^2 \kappa_k^{(j)} = 0$. Recall that $T_{j\alpha} = D^{(j)}(\vec{n}^{(\alpha)})$ equals the distance from the α th vertex to the j th facet. Direct computation yields

$$T = \frac{\sqrt{6}}{2} \begin{pmatrix} 3 & 0 & 0 & 1 \\ 0 & 3 & 0 & 1 \\ 0 & 0 & 3 & 1 \end{pmatrix} \quad (56)$$

with pseudoinverse

$$T^+ = \frac{2}{\sqrt{6}} \frac{1}{36} \begin{pmatrix} 11 & -1 & -1 \\ -1 & 11 & -1 \\ -1 & -1 & 11 \\ 3 & 3 & 3 \end{pmatrix}. \quad (57)$$

Since T has rank 3, its kernel is one-dimensional. One readily verifies that it is spanned by $(1, 1, 1, -3)^\top$. Consequently, the radicands in Eq. (31) admit the explicit

parametrization

$$T^+ \vec{D}(\vec{n}) + \vec{x} = \begin{pmatrix} \frac{n_0}{3} - \frac{1}{12} \\ \frac{n_1}{3} - \frac{1}{12} \\ \frac{n_2}{3} - \frac{1}{12} \\ \frac{1}{4} \end{pmatrix} + \xi \begin{pmatrix} 1 \\ 1 \\ 1 \\ -3 \end{pmatrix} = \begin{pmatrix} \frac{n_0 - z}{3} \\ \frac{n_1 - z}{3} \\ \frac{n_2 - z}{3} \\ z \end{pmatrix}, \quad (58)$$

where $z \equiv \frac{1}{4} - 3\xi$. This is the key structural simplification: the general representation Eq. (31) reduces the remaining nontrivial dependence of \mathcal{F} to a *single* scalar parameter z associated with $\ker(T)$. The ensuing approximation problem is therefore both low-dimensional and geometrically constrained.

C. Applying Eq. (31)

Because $|\vec{n}^{(1)}\rangle$, $|\vec{n}^{(2)}\rangle$, and $|\vec{n}^{(3)}\rangle$ each couple only to $|\vec{n}^{(4)}\rangle$ (and not to one another), the minimization over phases $\{\eta_\alpha\}$ in Eq. (31) is immediate; one admissible choice is $\eta_4 = -1$ and $\eta_1 = \eta_2 = \eta_3 = +1$. With the phases fixed, \mathcal{F} can be written as

$$\mathcal{F}[\vec{n}] = 2 + 2z - \frac{4\sqrt{6}}{3} \sum_{k=0}^2 \sqrt{\frac{n_k - z}{3}} \sqrt{z}, \quad (59)$$

where the remaining task is the minimization over z . In what follows, we denote by $\bar{z}(\vec{n})$ the minimizing value at \vec{n} .

a. A constrained, physics-informed approximation for \bar{z} . From the radicands in the previous subsection we have $0 \leq z \leq \min(n_0, n_1, n_2) \equiv z_{\max}(\vec{n})$. A central point of this proof of concept is that, once the representation Eq. (59) is available, constructing a useful approximation for \mathcal{F} reduces to proposing a plausible approximation for the *scalar* minimizer $\bar{z}(\vec{n})$ consistent with (i) facet behavior and (ii) regularity at symmetric points. We therefore make the simplifying ansatz that \bar{z} depends on \vec{n} only through z_{\max} and construct a function $\bar{z}(z_{\max})$ that matches these constraints.

On the facet $n_0 = 0$ (hence $z_{\max} = 0$) we necessarily have $\bar{z} = 0$. Moreover, moving slightly away from that facet, Eq. (59) becomes

$$\mathcal{F}[n_0, n_1, n_2] = 2 - \frac{4\sqrt{6}}{3} \left(\sqrt{\frac{n_1}{3}} + \sqrt{\frac{n_2}{3}} \right) \sqrt{z} + O(n_0), \quad (60)$$

since $z \leq n_0 \ll n_1, n_2$. At this level, the minimum is attained by choosing $z = n_0$, suggesting the boundary condition $\bar{z}'(0) = 1$. Importantly, the mechanism behind this behavior is precisely the one analyzed in Sec. V: the \sqrt{z} -term induces the characteristic repulsive tendency away from the facet, and therefore directly constrains the admissible shape of \bar{z} near $z_{\max} = 0$.

At the domain center, $z_{\max} = 1$ and $\vec{n} = (1, 1, 1)$, one finds from Eq. (59)

$$\mathcal{F}[1, 1, 1] = 2 + 2z - 4\sqrt{2}\sqrt{1-z}\sqrt{z}, \quad (61)$$

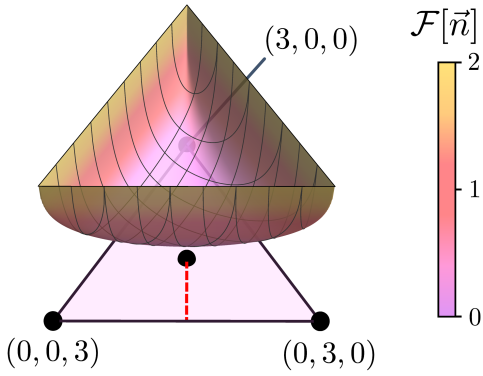


FIG. 9. Exact functional for the Bose-Hubbard model with $(d, N, P) = (3, 3, 0)$.

which is minimized at $z = \frac{1}{3}$. We therefore impose the four conditions

$$\begin{aligned} \bar{z}(0) &= 0 & \bar{z}'(0) &= 1 \\ \bar{z}(1) &= \frac{1}{3} & \bar{z}'(1) &= 0, \end{aligned} \quad (62)$$

where $\bar{z}'(1) = 0$ is chosen to ensure differentiability of the resulting approximate functional at $\vec{n} = (1, 1, 1)$.

The simplest polynomial satisfying Eq. (62) is

$$\bar{z}^{\text{approx}} = z_{\max} \left(\frac{z_{\max}^2}{3} - z_{\max} + 1 \right), \quad (63)$$

which yields an approximate functional (more precisely, an upper bound) when inserted into Eq. (59).

b. Validation against numerical minimization of z . For Fig. 9, we numerically minimize Eq. (59) over z and then plot the resulting exact \mathcal{F} . In Fig. 10, the exact numerical functional and minimizer \bar{z} are compared to their approximated counterparts obtained from Eq. (63) along the straight path from $(0, \frac{3}{2}, \frac{3}{2})$ to $(1, 1, 1)$. While \bar{z}^{approx} exhibits small deviations from the exact minimizer, the corresponding approximate functional is visually indistinguishable from the exact \mathcal{F} along that path.

The pointwise error of the approximate functional over the full domain is shown in Fig. 11a. The largest deviations occur near the line segments connecting $(1, 1, 1)$ to $(3, 0, 0)$, $(0, 3, 0)$, and $(0, 0, 3)$, and in their vicinity. Nevertheless, we find numerically that the maximum error is 0.024, which is only about 1% of $\max \mathcal{F}(\vec{n}) - \min \mathcal{F}(\vec{n})$ on the domain (see Fig. 9).

c. Impact on energies: accuracy of the induced variational problem. Since $\mathcal{F}^{\text{approx}}$ stays close to the exact functional throughout the domain, the corresponding approximate ground-state energy

$$E_{\text{approx}}[\vec{t}] = \min_{\vec{n}} (\vec{t} \cdot \vec{n} + \mathcal{F}^{\text{approx}}[\vec{n}]) \quad (64)$$

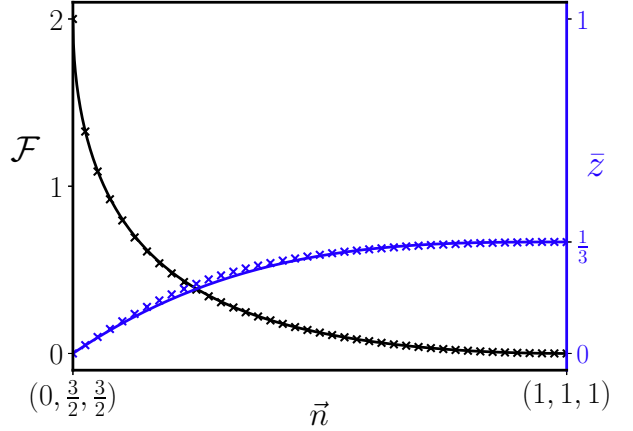
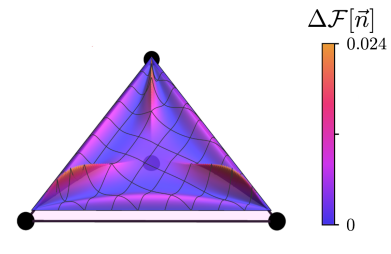
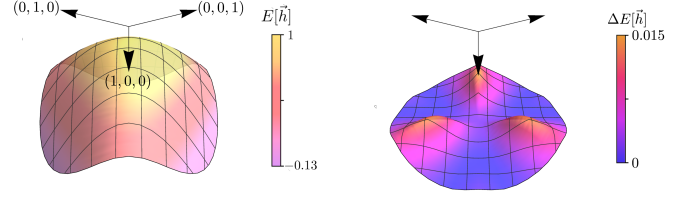


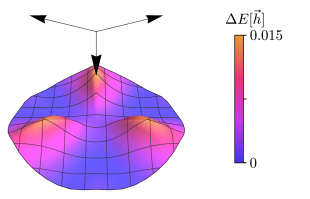
FIG. 10. Comparison between approximated \mathcal{F} and \bar{z} (solid curves) and the numerical values (cross markers) along the dotted line segment in Fig. 9.



(a) functional error



(b) exact ground state energy



(c) ground state energy error

FIG. 11. The error of our functional approximation by plugging Eq. (63) into Eq. (59) (top), along with the exact ground state energy (bottom left) and the respective error (bottom right). The arrows in the energy plots indicate directions in the 3-dimensional \vec{h} -space.

is expected to be accurate as well. Figure 11b displays the exact energy for the family of one-particle Hamiltonians

$$\vec{t}(r, \theta) = \begin{pmatrix} \frac{-1}{\sqrt{6}} & \frac{-1}{\sqrt{2}} \\ \frac{-1}{\sqrt{6}} & \frac{1}{\sqrt{2}} \\ \frac{2}{\sqrt{6}} & 0 \end{pmatrix} \begin{pmatrix} r \cos \theta \\ r \sin \theta \end{pmatrix} + \frac{1}{3} \begin{pmatrix} 1 \\ 1 \\ 1 \end{pmatrix}, \quad (65)$$

with $r \in [0, 1]$ and $\theta \in [0, 2\pi]$. (The last term merely adds a constant to the Hamiltonian and does not affect the physics.) Geometrically, this parameterizes a disk in the affine space $\{\vec{t} \mid t_0 + t_1 + t_2 = 1\} \subset \mathbb{R}^3$. The error $\Delta E[\vec{t}] \equiv E_{\text{approx}}[\vec{t}] - E[\vec{t}]$ is shown in Fig. 11c; over

the displayed parameter range, the approximate energy is again accurate to about 1% of $\max E[\vec{h}] - \min E[\vec{h}]$ on the disk.

To conclude, this example serves as a proof of concept that the fruitful geometric structure of $\text{dom}(\mathcal{F})$ and the BEC force can be exploited to construct sophisticated functional approximations in a controlled and transparent manner.

VII. SUMMARY AND CONCLUSION

In this work, we have developed a symmetry-adapted reduced density matrix functional theory (RDMFT) framework for interacting bosonic lattice systems. Building on the constrained-search formulation of RDMFT, we demonstrated that translational invariance, together with a fixed interaction \hat{W} , leads to a decisive simplification of the functional description: the basic functional variable reduces unambiguously from the full one-particle reduced density matrix $\hat{\gamma}$ to the momentum occupation number vector \vec{n} . As a result, the ground-state energy of translationally invariant lattice bosons can be described by a universal interaction functional defined solely on this reduced set of variables. This formulation is directly relevant for ultracold atomic gases, where momentum distributions are experimentally accessible and Bose-Einstein condensation admits a natural characterization within RDMFT through the Penrose-Onsager criterion.

A central result of the paper is that the structure of this universal functional is governed by the geometry of its domain, which is completely determined by one-body N -representability. We showed that the admissible set of momentum occupation numbers forms a reduced, symmetry-adapted convex polytope. By expressing the functional in coordinates adapted to the facets of this polytope, we derived a general form in which the dependence on the occupation numbers is dictated primarily by geometric considerations rather than by the detailed form of the interaction.

This geometric perspective has direct physical consequences. We demonstrated that the geometry of the representability domain enforces a universal boundary behavior of the functional: as the occupation number vector approaches any facet of the domain, the gradient of the functional diverges repulsively. This generalized BEC force extends earlier observations near the condensation vertex to arbitrary boundaries of the domain. Going beyond qualitative arguments, we derived a closed analytical expression for the corresponding repulsion strength. The resulting boundary behavior is therefore not a model-dependent feature but a structural consequence of the constrained-search formulation and of N -representability, and is expected to arise generically in interacting bosonic quantum systems.

Beyond its conceptual implications, the geometric form of the functional provides concrete guidance for the construction of approximations. The exact near-boundary

behavior imposes nontrivial constraints on admissible functionals, while at the same time suggesting a hierarchy of geometry-informed approximation schemes. We illustrated this strategy analytically for a few-site lattice system, demonstrating how exact geometric input can be combined with interaction-specific information in a controlled and transparent manner. This example serves as a proof of concept for a broader approximation program.

Taken together, our results show that spatial symmetry, N -representability, and the geometry of quantum states are intrinsically linked, as anticipated in Fig. 1, and jointly determine the structure of bosonic reduced density matrix functionals. While our explicit constructions were carried out for one-dimensional lattice systems, the generality of the geometric framework makes it clear that analogous results can be obtained for higher spatial dimensions and for bosons carrying additional internal degrees of freedom, such as spin. Moreover, several of the key insights derived here extend, at least qualitatively, to ensemble formulations, reflecting the general principle that functional theories are defined by two fundamental ingredients: a scope, specifying the class of physical systems under consideration, and a variational principle, such as the Rayleigh-Ritz principle for ground states or its ensemble generalizations for excited-state theories.

At a more fundamental level, our results suggest a shift in perspective on the choice of basic variables in functional theories. The decisive role played by the distances of \vec{n} to the facets of the representability domain indicates that it is often natural to reparameterize the functional not in terms of the density matrix or occupation numbers themselves, but in terms of their geometric distances to the boundary of the admissible set. Making this structure explicit provides direct physical insight, constrains admissible functional forms, and offers a principled starting point for systematic approximations. In this way, the present work closes a conceptual gap in bosonic RDMFT and lays the foundation for a geometry-driven approach to predictive functional theories of strongly correlated bosonic systems.

ACKNOWLEDGMENTS

We are grateful to Markus Penz for valuable feedback on the manuscript. We acknowledge financial support from the German Research Foundation (Grant SCHI 1476/1-1).

Appendix A: Derivation of the Generalized BEC Force

Here we present the derivation of the generalized BEC force without the simplex assumption. We adopt the notation that $I^{(j)}$ denotes all indices α for which the occupation number vector $\vec{n}^{(\alpha)}$ satisfies $D^{(j)}(\vec{n}^{(\alpha)}) = 0$. In other words, $I^{(j)}$ is the set of indices of all occupation

number vectors on facet j . The intuition is as follows: whenever a density \vec{n} approaches one of the facets, say $D^{(s)}(\vec{n}) = \epsilon \ll 1$, the wave function must assume a form such that the coefficients of configuration states $|\vec{n}^{(\alpha)}\rangle$ not on the facet approach zero at a rate proportional to $\sqrt{\epsilon}$. In this regime, the zeroth-order contribution to the functional arises from the configuration states on the facet, to which a correction of order $\sqrt{\epsilon}$ from facet-off-facet interactions is added. This latter term is the origin of the generalized BEC force.

Let \vec{n}^* be a point on facet s , i.e., $D^{(s)}(\vec{n}^*) = 0$. Let $|\Phi(\epsilon)\rangle$, with $\epsilon \in [0, \epsilon']$, be a curve such that $|\Phi(\epsilon)\rangle \mapsto \vec{n}^* + \epsilon \vec{\kappa}^{(s)}$, and such that $|\Phi(\epsilon)\rangle$ is a minimizer of the constrained search for each ϵ . That is,

$$\mathcal{F}[\vec{n}^* + \epsilon \vec{\kappa}^{(s)}] = \langle \Phi(\epsilon) | \hat{W} | \Phi(\epsilon) \rangle. \quad (\text{A1})$$

Write $|\Phi(\epsilon)\rangle = \sum_{\alpha} c_{\alpha}(\epsilon) |\vec{n}^{(\alpha)}\rangle$. We assume that the coefficients $c_{\alpha}(\epsilon)$ take the following form:

$$\begin{cases} c_{\alpha}(\epsilon) = p_{\alpha} + \epsilon q_{\alpha} + O(\epsilon^2), & \alpha \in I^{(s)}, \\ c_{\alpha}(\epsilon) = \sqrt{\epsilon} r_{\alpha} + O(\epsilon), & \alpha \notin I^{(s)}. \end{cases} \quad (\text{A2})$$

Equation (A2) requires some justification. Since $\langle \Phi(\epsilon) | \hat{n}_k | \Phi(\epsilon) \rangle$ depends linearly on each $|c_{\alpha}(\epsilon)|^2$, and only the ‘off-facet’ states, i.e., $|\vec{n}^{(\alpha)}\rangle$ with $\alpha \notin I^{(s)}$, can contribute to the deviation $\epsilon \vec{\kappa}^{(s)}$ from the facet, we must have $c_{\alpha}(\epsilon) \sim \sqrt{\epsilon}$ for $\alpha \notin I^{(s)}$, up to higher-order corrections in ϵ . On the other hand, it is not immediately clear that the ‘on-facet’ coefficients, i.e., $c_{\alpha}(\epsilon)$ with $\alpha \in I^{(s)}$, should not contain terms proportional to $\sqrt{\epsilon}$. Indeed, if $c_{\alpha}(0) = 0$, it is conceivable that $c_{\alpha}(\epsilon) \sim \sqrt{\epsilon}$ even if $\alpha \in I^{(s)}$. However, the vanishing of $c_{\alpha}(0)$ implies that the state $|\vec{n}^{(\alpha)}\rangle$ is decoupled from other states on the facet, so c_{α} does not contribute to the generalized BEC force.

Plugging Eq. (A2) into Eq. (A1) yields

$$\begin{aligned} \mathcal{F}[\vec{n}^* + \epsilon \vec{\kappa}^{(s)}] &= \sum_{\alpha, \beta \in I^{(s)}} p_{\alpha}^* p_{\beta} \langle \vec{n}^{(\alpha)} | \hat{W} | \vec{n}^{(\beta)} \rangle \\ &\quad + 2\sqrt{\epsilon} \operatorname{Re} \sum_{\alpha \in I^{(s)}, \beta \notin I^{(s)}} p_{\alpha}^* r_{\beta} \langle \vec{n}^{(\alpha)} | \hat{W} | \vec{n}^{(\beta)} \rangle + O(\epsilon). \end{aligned} \quad (\text{A3})$$

The coefficients p_{α} must be chosen so as to minimize the first term, and the result is simply $\mathcal{F}[\vec{n}^*]$. Similarly, the coefficients r_{α} are fixed by minimizing the second term. Observe that the phases are not frustrated: there is always a choice of phases that minimizes the expression.

Thus,

$$\begin{aligned} \frac{\mathcal{F}[\vec{n}^* + \epsilon \vec{\kappa}^{(s)}] - \mathcal{F}[\vec{n}^*]}{\sqrt{\epsilon}} &= -2 \sum_{\beta \notin I^{(s)}} |r_{\beta}| \left| \sum_{\alpha \in I^{(s)}} p_{\alpha}^* \langle \vec{n}^{(\alpha)} | \hat{W} | \vec{n}^{(\beta)} \rangle \right| \\ &= -2 \sum_{\beta \notin I^{(s)}} |r_{\beta}| \left| \langle \Phi^* | \hat{W} | \vec{n}^{(\beta)} \rangle \right|, \end{aligned} \quad (\text{A4})$$

where we have defined $|\Phi^* \rangle \equiv |\Phi(0)\rangle = \sum_{\alpha \in I^{(s)}} p_{\alpha} |\vec{n}^{(\alpha)}\rangle$. The quantities $|r_{\beta}|$ cannot be chosen arbitrarily: the condition $|\Phi(\epsilon)\rangle \mapsto \vec{n}^* + \epsilon \vec{\kappa}^{(s)}$ implies

$$\sum_{\alpha \in I^{(s)}} \vec{n}^{(\alpha)} (|p_{\alpha}|^2 + 2\epsilon \operatorname{Re} p_{\alpha}^* q_{\alpha}) + \epsilon \sum_{\alpha \notin I^{(s)}} \vec{n}^{(\alpha)} |r_{\alpha}|^2 = \vec{n}^* + \epsilon \vec{\kappa}^{(s)}, \quad (\text{A5})$$

and therefore

$$2\operatorname{Re} \sum_{\alpha \in I^{(s)}} \vec{n}^{(\alpha)} p_{\alpha}^* q_{\alpha} + \sum_{\alpha \notin I^{(s)}} \vec{n}^{(\alpha)} |r_{\alpha}|^2 = \vec{\kappa}^{(s)}. \quad (\text{A6})$$

Taking the dot product with $\vec{\kappa}^{(s)}$ and using $\vec{\kappa}^{(s)} \cdot \vec{n}^{(\alpha)} = -\mu^{(s)}$ for $\alpha \in I^{(s)}$, we obtain

$$-2\mu^{(s)} \operatorname{Re} \sum_{\alpha \in I^{(s)}} p_{\alpha}^* q_{\alpha} + \sum_{\alpha \notin I^{(s)}} |r_{\alpha}|^2 \vec{\kappa}^{(s)} \cdot \vec{n}^{(\alpha)} = |\vec{\kappa}^{(s)}|^2 = 1. \quad (\text{A7})$$

(Recall that we assumed $\vec{\kappa}^{(s)} \cdot \vec{\kappa}^{(s)} = 1$ at the beginning of Sec. V.) Normalization, $\langle \Phi(\epsilon) | \Phi(\epsilon) \rangle = 1$, implies

$$2\operatorname{Re} \sum_{\alpha \in I^{(s)}} p_{\alpha}^* q_{\alpha} = - \sum_{\alpha \notin I^{(s)}} |r_{\alpha}|^2, \quad (\text{A8})$$

which leads to

$$\sum_{\alpha \notin I^{(s)}} |r_{\alpha}|^2 D^{(s)}(\vec{n}^{(\alpha)}) = 1. \quad (\text{A9})$$

That is, the final line of Eq. (A4) must be minimized subject to the constraint (A9). This constrained minimization can be carried out explicitly and yields

$$\begin{aligned} \mathcal{G}[\vec{n}^*] &= \frac{\mathcal{F}[\vec{n}^* + \epsilon \vec{\kappa}^{(s)}] - \mathcal{F}[\vec{n}^*]}{\sqrt{\epsilon}} \\ &= -2 \left[\sum_{\alpha: D^{(s)}(\vec{n}^{(\alpha)}) > 0} \frac{\left| \langle \vec{n}^{(\alpha)} | \hat{W} | \Phi^* \rangle \right|^2}{D^{(s)}(\vec{n}^{(\alpha)})} \right]^{1/2}. \end{aligned} \quad (\text{A10})$$

[1] P. Hohenberg and W. Kohn, Inhomogeneous electron gas, *Phys. Rev.* **136**, B864 (1964).
[2] W. Kohn and L. J. Sham, Self-consistent equations including exchange and correlation effects, *Phys. Rev.* **140**, A1133 (1965).
[3] K. Burke, Perspective on density functional theory, *J. Chem. Phys.* **136**, 150901 (2012).
[4] A. D. Becke, Perspective: Fifty years of density-functional theory in chemical physics, *J. Chem. Phys.* **140**, 18A301 (2014).
[5] P. J. Hasnip, K. Refson, M. I. J. Probert, J. R. Yates, S. J. Clark, and C. J. Pickard, Density functional theory in the solid state, *Philos. Trans. R. Soc. Math. Phys. Eng. Sci.* **372**, 20130270 (2014).
[6] T. L. Gilbert, Hohenberg-Kohn theorem for nonlocal external potentials, *Phys. Rev. B* **12**, 2111 (1975).

[7] R. A. Donnelly and R. G. Parr, Elementary properties of an energy functional of the first-order reduced density matrix, *J. Chem. Phys.* **69**, 4431 (1978).

[8] K. Pernal and K. J. H. Giesbertz, Reduced density matrix functional theory (RDMFT) and linear response time-dependent RDMFT (TD-RDMFT), in *Density-Functional Methods for Excited States*, Vol. 368, edited by N. Ferré, M. Filatov, and M. Huix-Rotllant (Springer International Publishing, Cham, 2015) pp. 125–183.

[9] G. Zumbach and K. Maschke, Density-matrix functional theory for the N-particle ground state, *J. Chem. Phys.* **82**, 5604 (1985).

[10] R. Schade, E. Kamil, and P. Blöchl, Reduced density-matrix functionals from many-particle theory, *Eur. Phys. J. Spec. Top.* **226**, 2677 (2017).

[11] C. Schilling, Communication: Relating the pure and ensemble density matrix functional, *The Journal of Chemical Physics* **149**, 231102 (2018).

[12] K. J. H. Giesbertz and M. Ruggenthaler, One-body reduced density-matrix functional theory in finite basis sets at elevated temperatures, *Phys. Rep.* **806**, 1 (2019).

[13] C. Schilling and S. Pittalis, Ensemble reduced density matrix functional theory for excited states and hierarchical generalization of pauli's exclusion principle, *Phys. Rev. Lett.* **127**, 023001 (2021).

[14] D. Gibney, J.-N. Boyn, and D. A. Mazziotti, Density functional theory transformed into a one-electron reduced-density-matrix functional theory for the capture of static correlation, *J. Phys. Chem. Lett.* **13**, 1382 (2022).

[15] J. Liebert, *Reduced Density Matrix Functional Theory for Bosons: Foundations and Applications*, Master's thesis, LMU Munich (2021), arXiv:2205.02635 [cond-mat].

[16] J. Liebert, F. Castillo, J.-P. Labbé, and C. Schilling, Foundation of one-particle reduced density matrix functional theory for excited states, *J. Chem. Theory Comput.* **18**, 124 (2022).

[17] M. Rodríguez-Mayorga, K. Giesbertz, and L. Visscher, Relativistic reduced density matrix functional theory, *SciPost Chem.* **1**, 004 (2022).

[18] J. Liebert and C. Schilling, An exact one-particle theory of bosonic excitations: from a generalized Hohenberg–Kohn theorem to convexified n -representability, *New J. Phys.* **25**, 013009 (2023).

[19] J. Liebert, A. Y. Chaou, and C. Schilling, Refining and relating fundamentals of functional theory, *J. Chem. Phys.* **158**, 214108 (2023).

[20] J. Liebert, *Quantum Information Theoretical Approach to Functional Theories*, Phd thesis, LMU Munich (2025).

[21] H. R. Fredheim and S. Kvaal, Reduced density matrix functional theory and a reduced formulation of density functional theory (2025), arXiv:2510.12242 [math-ph].

[22] C. Schilling and R. Schilling, Diverging exchange force and form of the exact density matrix functional, *Phys. Rev. Lett.* **122**, 013001 (2019).

[23] J. Ciosłowski, Z. É. Mihálka, and Á. Szabados, Bilinear constraints upon the correlation contribution to the electron–electron repulsion energy as a functional of the one-electron reduced density matrix, *J. Chem. Theory Comput.* **15**, 4862 (2019).

[24] T. Maciążek, Repulsively diverging gradient of the density functional in the reduced density matrix functional theory, *New J. Phys.* **23**, 113006 (2021).

[25] R. López-Sandoval and G. M. Pastor, Density-matrix functional theory of the Hubbard model: An exact numerical study, *Phys. Rev. B* **61**, 1764 (2000).

[26] W. Töws, M. Saubanère, and G. M. Pastor, Density-matrix functional theory of strongly correlated fermions on lattice models and minimal-basis Hamiltonians, *Theor. Chem. Acc.* **133**, 1422 (2013).

[27] A. J. Cohen and P. Mori-Sánchez, Landscape of an exact energy functional, *Phys. Rev. A* **93**, 042511 (2016).

[28] C. L. Benavides-Riveros, J. Wolff, M. A. L. Marques, and C. Schilling, Reduced density matrix functional theory for bosons, *Phys. Rev. Lett.* **124**, 180603 (2020).

[29] A. M. K. Müller, Explicit approximate relation between reduced two- and one-particle density matrices, *Phys. Lett. A* **105**, 446 (1984).

[30] S. Goedecker and C. J. Umrigar, Natural orbital functional for the many-electron problem, *Phys. Rev. Lett.* **81**, 866 (1998).

[31] K. Yasuda, Correlation energy functional in the density-matrix functional theory, *Phys. Rev. A* **63**, 032517 (2001).

[32] M. A. Buijse and E. J. Baerends, An approximate exchange-correlation hole density as a functional of the natural orbitals, *Mol. Phys.* **100**, 401 (2002).

[33] R. López-Sandoval and G. M. Pastor, Density-matrix functional theory of strongly correlated lattice fermions, *Phys. Rev. B* **66**, 155118 (2002).

[34] C. Kollmar and B. A. Heß, A new approach to density matrix functional theory, *J. Chem. Phys.* **119**, 4655 (2003).

[35] R. López-Sandoval and G. M. Pastor, Interaction-energy functional for lattice density functional theory: Applications to one-, two-, and three-dimensional Hubbard models, *Phys. Rev. B* **69**, 085101 (2004).

[36] O. Gritsenko, K. Pernal, and E. J. Baerends, An improved density matrix functional by physically motivated repulsive corrections, *J. Chem. Phys.* **122**, 204102 (2005).

[37] M. Piris, Natural orbital functional theory, in *Reduced-Density-Matrix Mechanics: With Application to Many-Electron Atoms and Molecules* (John Wiley & Sons, Ltd, 2007) Chap. 14, pp. 385–427.

[38] M. Piris, X. Lopez, F. Ruipérez, J. M. Matxain, and J. M. Ugalde, A natural orbital functional for multiconfigurational states, *J. Chem. Phys.* **134**, 164102 (2011).

[39] W. Töws and G. M. Pastor, Spin-polarized density-matrix functional theory of the single-impurity Anderson model, *Phys. Rev. B* **86**, 245123 (2012).

[40] I. Mitxelena, M. Piris, and M. Rodríguez-Mayorga, On the performance of natural orbital functional approximations in the Hubbard model, *J. Phys.: Condens. Matter* **29**, 425602 (2017).

[41] C. L. Benavides-Riveros and M. A. L. Marques, Static correlated functionals for reduced density matrix functional theory, *Eur. Phys. J. B* **91**, 133 (2018).

[42] K. J. H. Giesbertz, A.-M. Uimonen, and R. van Leeuwen, Approximate energy functionals for one-body reduced density matrix functional theory from many-body perturbation theory, *Eur. Phys. J. B* **91**, 282 (2018).

[43] R. van Meer, O. V. Gritsenko, and E. J. Baerends, A non-JKL density matrix functional for intergeminal cor-

relation between closed-shell geminals from analysis of natural orbital configuration interaction expansions, *J. Chem. Phys.* **148**, 104102 (2018).

[44] M. Piris, Natural orbital functional for multiplets, *Phys. Rev. A* **100**, 032508 (2019).

[45] B. Senjean, S. Yalouz, N. Nakatani, and E. Fromager, Reduced density matrix functional theory from an ab initio seniority-zero wave function: Exact and approximate formulations along adiabatic connection paths, *Phys. Rev. A* **106**, 032203 (2022).

[46] S. Di Sabatino, J. Koskelo, J. A. Berger, and P. Romaniello, Introducing screening in one-body density matrix functionals: Impact on charged excitations of model systems via the extended Koopmans' theorem, *Phys. Rev. B* **105**, 235123 (2022).

[47] J. Wang and E. J. Baerends, Self-consistent-field method for correlated many-electron systems with an entropic cumulant energy, *Phys. Rev. Lett.* **128**, 013001 (2022).

[48] M. Irimia, Y. Wang, Y. Fei, and J. Wang, Self-consistent-field method for correlation calculation within density-matrix-functional theory, *Phys. Rev. A* **108**, 052818 (2023).

[49] J. Liebert and C. Schilling, Deriving density-matrix functionals for excited states, *SciPost Phys.* **14**, 120 (2023).

[50] M. Piris, Advances in approximate natural orbital functionals: From historical perspectives to contemporary developments, in *Advances in Quantum Chemistry*, Vol. 90 (Elsevier, 2024) pp. 15–66.

[51] S. Sharma, J. K. Dewhurst, N. N. Lathiotakis, and E. K. U. Gross, Reduced density matrix functional for many-electron systems, *Phys. Rev. B* **78**, 201103 (2008).

[52] N. N. Lathiotakis, S. Sharma, N. Helbig, J. K. Dewhurst, M. a. L. Marques, F. Eich, T. Baldsiefen, A. Zacarias, and E. K. U. Gross, Discontinuities of the chemical potential in reduced density matrix functional theory, *Z. Phys. Chem.* **224**, 467 (2010).

[53] Y. Lemke, J. Kussmann, and C. Ochsenfeld, Efficient integral-direct methods for self-consistent reduced density matrix functional theory calculations on central and graphics processing units, *J. Chem. Theory Comput.* **18**, 4229 (2022).

[54] N. G. Cartier and K. J. H. Giesbertz, Exploiting the hessian for a better convergence of the SCF-RDMFT procedure, *J. Chem. Theory Comput.* **20**, 3669 (2024).

[55] Y.-F. Yao and N. Q. Su, Enhancing reduced density matrix functional theory calculations by coupling orbital and occupation optimizations, *J. Phys. Chem. A* **128**, 7669 (2024).

[56] M. Vladaj, Q. Marécat, B. Senjean, and M. Saubanère, Variational minimization scheme for the one-particle reduced density matrix functional theory in the ensemble N-representability domain, *J. Chem. Phys.* **161**, 074105 (2024).

[57] I. Bloch, J. Dalibard, and W. Zwerger, Many-body physics with ultracold gases, *Rev. Mod. Phys.* **80**, 885 (2008).

[58] M. H. Anderson, J. R. Ensher, M. R. Matthews, C. E. Wieman, and E. A. Cornell, Observation of Bose-Einstein condensation in a dilute atomic vapor, *Science* **269**, 198 (1995).

[59] O. Penrose and L. Onsager, Bose-Einstein condensation and liquid helium, *Phys. Rev.* **104**, 576 (1956).

[60] C. C. Bradley, C. A. Sackett, J. J. Tollett, and R. G. Hulet, Evidence of Bose-Einstein condensation in an atomic gas with attractive interactions, *Phys. Rev. Lett.* **75**, 1687 (1995).

[61] K. B. Davis, M. O. Mewes, M. R. Andrews, N. J. van Druten, D. S. Durfee, D. M. Kurn, and W. Ketterle, Bose-Einstein condensation in a gas of sodium atoms, *Phys. Rev. Lett.* **75**, 3969 (1995).

[62] I. Bloch, Ultracold quantum gases in optical lattices, *Nat. Phys.* **1**, 23 (2005).

[63] I. Bloch, J. Dalibard, and S. Nascimbène, Quantum simulations with ultracold quantum gases, *Nat. Phys.* **8**, 267 (2012).

[64] C. Gross and I. Bloch, Quantum simulations with ultracold atoms in optical lattices, *Science* **357**, 995 (2017).

[65] F. Schäfer, T. Fukuhara, S. Sugawa, Y. Takasu, and Y. Takahashi, Tools for quantum simulation with ultracold atoms in optical lattices, *Nat. Rev. Phys.* **2**, 411 (2020).

[66] D. Jaksch, C. Bruder, J. I. Cirac, C. W. Gardiner, and P. Zoller, Cold bosonic atoms in optical lattices, *Phys. Rev. Lett.* **81**, 3108 (1998).

[67] D. Jaksch and P. Zoller, The cold atom Hubbard toolbox, *Ann. Phys. Special Issue*, **315**, 52 (2005).

[68] M. Greiner, O. Mandel, T. Esslinger, T. W. Hänsch, and I. Bloch, Quantum phase transition from a superfluid to a Mott insulator in a gas of ultracold atoms, *Nature* **415**, 39 (2002).

[69] I. Bloch and M. Greiner, The superfluid-to-Mott insulator transition and the birth of experimental quantum simulation, *Nat. Rev. Phys.* **4**, 739 (2022).

[70] M. Levy, Universal variational functionals of electron densities, first-order density matrices, and natural spin-orbitals and solution of the v-representability problem, *Proc. Natl. Acad. Sci.* **76**, 6062 (1979).

[71] S. M. Valone, Consequences of extending 1-matrix energy functionals from pure-state representable to all ensemble representable 1 matrices, *J. Chem. Phys.* **73**, 1344 (1980).

[72] R. E. Borland and K. Dennis, The conditions on the one-matrix for three-body fermion wavefunctions with one-rank equal to six, *J. Phys. B: Atom. Mol. Phys.* **5**, 7 (1972).

[73] A. A. Klyachko, Quantum marginal problem and N-representability, *J. Phys.: Conf. Ser.* **36**, 72 (2006).

[74] M. Altunbulak and A. Klyachko, The Pauli principle revisited, *Commun. Math. Phys.* **282**, 287 (2008).

[75] M. Altunbulak, *The Pauli Principle, Representation Theory, and Geometry of Flag Varieties*, Ph.D. thesis, Bilkent University (2008).

[76] T. Maciążek, A. Sawicki, D. Gross, A. Lopes, and C. Schilling, Implications of pinned occupation numbers for natural orbital expansions. II: Rigorous derivation and extension to non-fermionic systems, *New J. Phys.* **22**, 023002 (2020).

[77] E. K. U. Gross, L. N. Oliveira, and W. Kohn, Density-functional theory for ensembles of fractionally occupied states. I. Basic formalism, *Phys. Rev. A* **37**, 2809 (1988).

[78] L. Ding, C.-L. Hong, and C. Schilling, Ground and excited states from ensemble variational principles, *Quantum* **8**, 1525 (2024).

[79] A. K. Theophilou, The energy density functional formalism for excited states, *J. Phys. C: Solid State Phys.* **12**, 5419 (1979).

[80] E. K. U. Gross, L. N. Oliveira, and W. Kohn, Density-functional theory for ensembles of fractionally occupied states. I. Basic formalism, *Phys. Rev. A* **37**, 2809 (1988).

[81] L. N. Oliveira, E. K. U. Gross, and W. Kohn, Density-functional theory for ensembles of fractionally occupied states. II. Application to the He atom, *Phys. Rev. A* **37**, 2821 (1988).

[82] P.-F. Loos and E. Fromager, A weight-dependent local correlation density-functional approximation for ensembles, *J. Chem. Phys.* **152**, 214101 (2020).

[83] E. Fromager, Individual correlations in ensemble density functional theory: State- and density-driven decompositions without additional Kohn-Sham systems, *Phys. Rev. Lett.* **124** (2020).

[84] T. Gould and L. Kronik, Ensemble generalized Kohn-Sham theory: The good, the bad, and the ugly, *J. Chem. Phys.* **154**, 094125 (2021).

[85] F. Cernatic, B. Senjean, V. Robert, and E. Fromager, Ensemble density functional theory of neutral and charged excitations, *Top. Curr. Chem.* **280**, 4 (2022).

[86] S. Giarrusso and P.-F. Loos, Exact excited-state functionals of the asymmetric Hubbard dimer, *J. Phys. Chem. Lett.* **14**, 8780 (2023).

[87] T. R. Scott, J. Kozlowski, S. Crisostomo, A. Pribram-Jones, and K. Burke, Exact conditions for ensemble density functional theory, *Phys. Rev. B* **109**, 195120 (2024).

[88] T. Gould and S. Pittalis, Local density approximation for excited states, *Phys. Rev. X* **14**, 041045 (2024).

[89] E. Fromager, Ensemble density functional theory of ground and excited energy levels, *J. Phys. Chem. A* **129**, 1143 (2025).

[90] F. Cernatic, P.-F. Loos, B. Senjean, and E. Fromager, Neutral electronic excitations and derivative discontinuities: An extended n -centered ensemble density functional theory perspective, *Phys. Rev. B* **109**, 235113 (2024).

[91] J. Liebert, T. Maciazeck, and C. Schilling, A spin-faithful functional theory for strongly correlated electrons, forthcoming (2025).

[92] J. Liebert, T. Maciazeck, and C. Schilling, How to incorporate symmetries in functional theories, forthcoming (2025).

[93] G. Günter, H. Schempp, M. Robert-de Saint-Vincent, V. Gavryusev, S. Helmrich, C. S. Hofmann, S. Whitlock, and M. Weidemüller, Observing the dynamics of dipole-mediated energy transport by interaction-enhanced imaging, *Science* **342**, 954 (2013).

[94] H. Schempp, G. Günter, S. Wüster, M. Weidemüller, and S. Whitlock, Correlated exciton transport in Rydberg-dressed-atom spin chains, *Phys. Rev. Lett.* **115**, 093002 (2015).

[95] M. A. L. Marques and N. N. Lathiotakis, Empirical functionals for reduced-density-matrix-functional theory, *Phys. Rev. A* **77**, 032509 (2008).

[96] M. Piris, Global natural orbital functional: Towards the complete description of the electron correlation, *Phys. Rev. Lett.* **127**, 233001 (2021).

[97] J. Schmidt, M. Fadel, and C. L. Benavides-Riveros, Machine learning universal bosonic functionals, *Phys. Rev. Res.* **3**, L032063 (2021).

[98] J. Liebert and C. Schilling, Functional theory for Bose-Einstein condensates, *Phys. Rev. Res.* **3**, 013282 (2021).

[99] C. Schilling, C. L. Benavides-Riveros, A. Lopes, T. Maciązeck, and A. Sawicki, Implications of pinned occupation numbers for natural orbital expansions: I. Generalizing the concept of active spaces, *New J. Phys.* **22**, 023001 (2020).

[100] C. Schilling, Hubbard model: Pinning of occupation numbers and role of symmetries, *Phys. Rev. B* **92**, 155149 (2015).

[101] C. Schilling, C. L. Benavides-Riveros, and P. Vrana, Reconstructing quantum states from single-party information, *Phys. Rev. A* **96**, 052312 (2017).

[102] J. Cioslowski, O. M. Brown, and T. Maciazeck, Natural orbitals and their occupation numbers for free anyons in the magnetic gauge, *Phys. Rev. A* **109**, 023316 (2024).

[103] J. M. Danskin, The theory of max-min, with applications, *SIAM J. Appl. Math.* **14**, 641 (1966), 2946123.